Rapid generation of both high- and low-$\delta^{18}O$, large-volume silicic magmas at the Timber Mountain/Oasis Valley caldera complex, Nevada

Ilya N. Bindeman†
John W. Valley
Department of Geology and Geophysics, University of Wisconsin, 1215 West Dayton Street, Madison, Wisconsin 53706, USA

ABSTRACT

We present an oxygen isotope and petrologic study of four voluminous, zoned ash-flow sheets of the Southwestern Nevada Volcanic Field (SWNVF): Topopah Spring (TS, >1200 km³, 12.8 Ma), Tiva Canyon (TC, 1000 km³, 12.7 Ma), Rainier Mesa (RM, 1200 km³, 11.6 Ma), and Ammonia Tanks (AT, 900 km³, 11.45 Ma). The $\delta^{18}O$ values of quartz, sanidine, sphene, magnetite, and zircons in rhyolites and latites of each tuff were measured and used to estimate $\delta^{18}O$(melt) at 700–900 °C. Temperatures were determined by $\Delta^{18}O$(quartz-magnetite) and Fe-Ti thermometers. Each tuff is characterized by a distinct range of $\delta^{18}O$(melt): 8.0–9.0‰ (TS), 7.1–7.8‰ (TC), 7.4–8.6‰ (RM), and 5.4–6.0‰ (AT), with higher $\delta^{18}O$ values for rhyolites in each unit. The distinct $\delta^{18}O$ of rhyolitic versus latitic portions of each tuff suggests that they can not be related by in situ fractionation and assimilation in a single zoned magma chamber. It is more likely that latite and rhyolite represent two magmas that were juxtaposed prior to eruption. Low-$\delta^{18}O$ AT and normal-$\delta^{18}O$ TC tuffs were erupted from the same nested caldera complex only 100–150 k.y. after eruption of voluminous high-$\delta^{18}O$ TS and RM magmas, respectively. These short time intervals, distinct $\delta^{18}O$, $^{87}Sr/^{86}Sr_i$, and ε_{Nd} of each tuff, the same loci of their eruption, and energy-constrained assimilation modeling suggest that TS, TC, RM, and AT represent independent magma batches that were rapidly generated, fractionated, and erupted from shallow, sheet-like magma chambers. Such geometry is a result of extensional tectonics in the Basin and Range province, and it favors nearly total evacuation of the magma chamber during a single eruption. Each silicic magma unit was generated by a shallow influx of new mafic magma that melted $^{18}O/^{16}O$-depleted (as in the case of AT) or $^{18}O/^{16}O$-enriched (RM, TS) rocks. The AT tuff and associated pre- and post-caldera lavas are 2.5‰ lower in $\delta^{18}O$ than in the RM tuff and represent the largest known low $\delta^{18}O$ magma. We find that all units of the AT cycle contain isotopically zoned zircons that have up to 2‰ core-to-rim zoning and correspondingly smaller, out-of-equilibrium quartz-zircon and melt-zircon fractionations. Air-abraded cores of quartz and sphene do not preserve any $\delta^{18}O$ zoning. The higher-$\delta^{18}O$ zircon cores in low-$\delta^{18}O$ magmas of SWNVF are similar to zoned zircons in low-$\delta^{18}O$ lavas at Yellowstone. In both places, normal-$\delta^{18}O$ zircons have been inherited from precursor volcanic rocks in that the matrix suffered depletion in $\delta^{18}O$ (down to +4% to +5% according to AFC modeling), but zircons and quartz survived hydrothermal alteration. These precursor rocks were later rapidly remelted to form low-$\delta^{18}O$ melt and caused progressive exchange of oxygen with normal-$\delta^{18}O$ zircon and quartz xenocrysts. Based on modeling of oxygen diffusion in zircon and quartz, the time between xenocryst entrapment and eruption is estimated to be 10^4 yr in SWNVF versus 10^3 yr for Yellowstone. We suggest that zircon recycling is a common feature of low-$\delta^{18}O$ magmas worldwide and is a signature of nearly total remelting of hydrothermally altered roof rocks, in hot-spot (Yellowstone) and in extensional (SWNVF) environments.

Keywords: Paintbrush tuff, Timber Mountain tuff, oxygen isotopes, isotope zoning, zircon, zone refinement melting.

INTRODUCTION

Timber Mountain/Oasis Valley Caldera Complex

The Timber Mountain/Oasis Valley volcanic center of the Southwestern Nevada Volcanic Field (SWNVF) is one of the largest centers of silicic magmatism in the western United States. The center consists mostly of zoned silicic ash-flow sheets (16 Ma to younger than 9 Ma); the volcanic eruption produced a group of nested calderas in the same lithospheric block (Fig. 1). The magmatic activity in SWNVF started at ca. 16 Ma and was likely associated with extension-related tectonism in the Great Basin, which was framed by the Late Proterozoic to Paleozoic metasedimentary rocks overlying the Precambrian basement (Christiansen et al., 1977; Byers et al., 1989). The 16–13 Ma silicic volcanics are less exposed and are overlain by younger tuffs and lavas. Tuffs of Paintbrush (12.8–12.7 Ma) and Timber Mountain (11.6–11.45 Ma) groups are the most voluminous and regionally abundant, and these are the primary focus of the present paper. Paintbrush Group tuffs: Topopah Spring (TS, >1200 km³, 12.8 Ma), Tiva Canyon (TC, 1000 km³, 12.7 Ma), and Timber Mountain Group tuffs: Rainier Mesa (RM, 1200 km³,11.6 Ma), and Ammonia Tanks (AT, 900 km³, 11.45 Ma) are related to four major caldera-forming events in the same general area (Fig. 1). Significantly, the $^{40}Ar/^{39}Ar$ ages of sanidine in each tuff unit (Sawyer et al., 1994; Huysken et al., 2001) demonstrate that only 100 k.y. separate TS from TC, and 150 k.y. separate RM from AT, two subsequent caldera-forming eruptions of each Paint-

†E-mail: inbindem@geology.wisc.edu.

GSA Bulletin; May 2003; v. 115; no. 5; p. 581–595; 10 figures; 2 tables; Data Repository item 2003066.

For permission to copy, contact editing@geosociety.org
© 2003 Geological Society of America

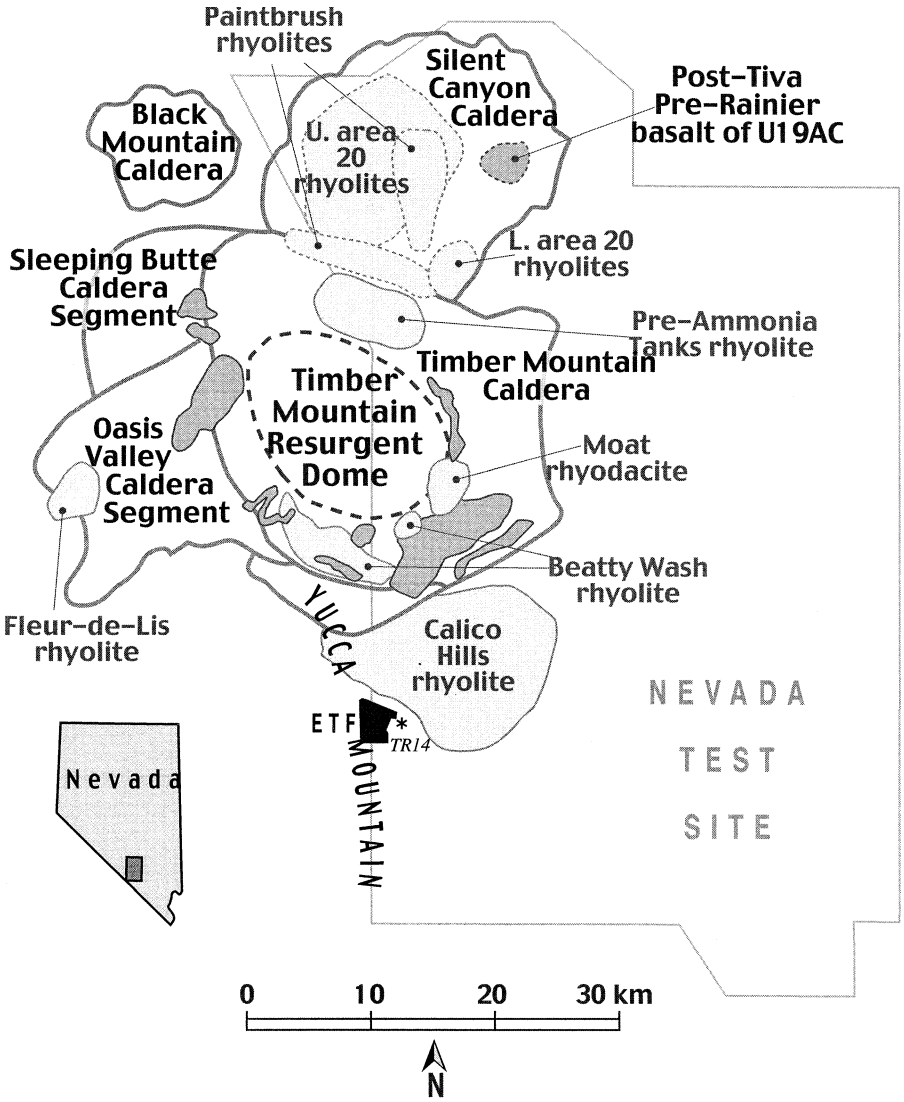

Figure 1. Map of the Timber Mountain/Oasis Valley caldera complex of the Southwestern Nevada Volcanic Field (SWNVF). Caldera rims for the four ash-flow sheets overlap. Eruptions of Paintbrush Group (Topopah Spring, Tiva Canyon tuffs, 12.8–12.7 Ma, >2200 km³), and Timber Mountain Group (Rainier Mesa and Ammonia Tanks tuffs, 11.6–11.45 Ma, >2200 km³) resulted in formation of Oasis Valley and Timber Mountain Calderas, respectively (Byers et al., 1976a; Christiansen et al., 1977). Smaller volume rhyolitic and basaltic (unmarked darker gray) lavas erupted following caldera collapses. Yucca Mountain is made of Topopah Spring and Tiva Canyon tuffs. ETF (Exploratory Tunnel Facility for long-term storage of nuclear waste) and TR-14 (Trench-14) are shown.

brush and Timber Mountain cycles. These relatively short time intervals and large volume of eruptions are critical geological constraints for understanding the petrogenesis of these magmas. Table 1 summarizes the mineralogy and chemical composition and presents the location of samples studied in this paper.

Each of these four ash-flow sheets (here called tuffs for brevity) is zoned in composition and phenocryst content, with smaller-volume crystal-rich (15%–25%) latitic portions residing on top of voluminous crystal-poor (1%–15%) rhyolitic portions (Table 1, Warren et al., 1989). Such stratigraphic sequences are traditionally interpreted to represent inverted stratigraphy of the magma chamber, implying that the position of latites and rhyolites was reverse in the magma chamber prior to eruption (e.g., Lipman, 1984). Pumice clast compositions and Fe-Ti oxide equilibration temperatures are continuously correlated in each tuff unit (Lipman et al., 1966, Lipman, 1971; Mills et al., 1997) and reflect compositional and temperature zoning in preclimactic magma chambers. Studies of melt inclusions in sanidine and quartz phenocrysts in rhyolitic and latitic portions of TS, RM, and AT tuffs (Vogel and Aines, 1996) demonstrate that volatile content increased upward (toward rhyolites) in magma chambers. Despite wide variations in composition and temperatures in each tuff unit, there is a small compositional gap at ~65 wt% SiO_2 (Mills et al., 1997) separating rhyodacitic to high-silica rhyolitic (~67–76 wt% SiO_2), and basaltic to latitic chemical groups (53–65 wt% SiO_2), although most mafic pumices are rare (Schuraytz et al., 1989; Flood et al., 1989; Warren et al., 1989, 2000).

A remarkable feature of AT and TC tuffs is that they are depleted in $^{18}O/^{16}O$ ratio with respect to preceding high-$\delta^{18}O$ in TS and RM tuffs, respectively (Friedman et al., 1974; Lipman and Friedman, 1975). The $\delta^{18}O$ values of AT tuff and of pre-AT and post-AT lavas are 2.5‰ lower than the $\delta^{18}O$ values of RM tuff and 1.5‰ lower than $\delta^{18}O$ values attainable by silicic magmas derived by fractionation of mantle-derived basalt (e.g., Harris et al., 2000; Eiler, 2001). Therefore, rocks of the Ammonia Tanks cycle are low-$\delta^{18}O$ magmas in the absolute sense, and AT tuff is the largest volume of low $\delta^{18}O$ magma to our knowledge.

Objectives of the Present Study

This work is a laser fluorination-based oxygen isotope study of phenocrysts in the four major zoned ash-flow sheets and in intracaldera lavas at the SWNVF. Our interest in the SWNVF is both scientific and practical. The scientific goal is to understand the genesis of large volume, compositionally zoned magmas having distinct $\delta^{18}O$ values (both low-$\delta^{18}O$ and high-$\delta^{18}O$). In a parallel study of quartz and zircon from Yellowstone rhyolites, we discovered isotopic zoning in single crystals, which allowed us to constrain the time scale and the mechanism of genesis of low-$\delta^{18}O$ magma (Bindeman and Valley, 2001). Comparison with Yellowstone is warranted because both at Yellowstone and at SWNVF there is a similar time interval of ca. 100 ka after eruption of normal-$\delta^{18}O$ and appearance of low-$\delta^{18}O$ magmas. In the present paper, we performed analyses of $\delta^{18}O$ in individual phenocrysts and refractory minerals (zircon, sphene, magnetite), which allow us to apply oxygen isotope thermometry and best estimate magmatic $\delta^{18}O$(melt) values. This provides the basis for understanding the extent of subsequent hydrothermal alteration and postmag-

TABLE 1. CHEMICAL COMPOSITION AND PHENOCRYST CONTENT OF TUFFS FROM TIMBER MOUNTAIN/OASIS VALLEY CALDERA COMPLEX

No.	Sample identification	Unit	Phenocrysts		SiO_2 (%)	TiO_2 (%)	Al_2O_3 (%)	Fe_2O_3 (%)	MnO (%)	MgO (%)	CaO (%)	Na_2O (%)	K_2O (%)	P_2O_5 (%)	Cr_2O_3 (%)	LOI (%)	Sum (%)	Rb (ppm)	Sr (ppm)	Y (ppm)	Nb (ppm)	Ba (ppm)	Zr (ppm)	Rb/Sr	"T, §°C" Zrc sat
			Vol%	Abundance†																					
1	99TM–11	"TS, lower"	3	SPBHCSpZMI	76.4	0.099	12.3	1.14	0.06	0.14	0.69	3.70	4.71	0.02	0.02	0.85	100.1	173	28	37	24	139	131	6.2	769
2	99TM–10	"TS, upper"	16	PSQBHCSpZMI	67.3	0.423	15.7	2.32	0.10	0.46	1.83	4.61	5.63	0.09	<0.01	0.70	99.2	102	193	28	15	2330	653	0.5	896
3	99TM–7	"TC, lower"	4	SPBHCSpZM	73.4	0.145	12.5	1.18	0.10	0.35	0.66	3.84	4.46	0.02	0.01	3.10	99.8	177	39	44	29	127	224	4.5	765
4	99TM–12	"TC, upper"	11	PSBHCSpZMI	67.0	0.393	14.5	1.96	0.11	0.72	2.98	4.66	5.18	0.08	0.01	2.35	99.9	111	101	34	18	768	566	1.1	852
5	99TM–13	"RM, lower"	16	SQPBHCSpZMIO	76.1	0.115	12.4	0.90	0.06	0.06	0.46	3.21	4.55	0.02	0.02	2.2	100.1	240	19	39	32	108	97	12.6	757
6	99TM–14	"RM, lower"		SQPBHCSpZMI	74.5	0.135	13.4	1.03	0.05	0.13	0.53	2.62	4.87	0.02	0.01	2.95	100.2	173	24	28	24	118	110	7.2	777
7	99TM–16	"RM, upper"	23	PSQBHCSpZMIO	76.8	76.8	12.4	1.19	0.05	0.14	0.62	3.58	4.85	0.03	0.02	0.30	100.2	126	55	22	19	235	169	2.3	797
8	99TM–26	"RM, upper"		PSQBHCSpZMI	68.7	0.366	14.6	3.30	0.15	0.25	0.74	5.15	5.24	0.06	<0.01	0.30	98.9	185	39	67	68	301	838	4.7	932
9	FB18D1–3‡	"RM, upper"	35	PSBHCSpZMI	67.9	0.274	13.5	1.42	0.11	0.40	1.52	3.17	6.18	0.02	ND	5.48	100.0	133	1239	ND	ND	3163	1424	0.1	994
10	99TM–24	Pre-AT	2	SPQHCSpZMI	75.5	0.124	11.8	0.96	0.08	0.07	0.41	3.69	4.37	0.02	0.03	3.00	100.1	228	11	37	39	82	135	20.7	776
11	99TM–15	"AT, lower"	14	SQPBHCSpZMI	75.7	0.184	12.6	1.20	0.08	0.21	0.61	4.00	4.89	0.06	0.02	0.60	100.2	188	49	39	33	222	215	3.8	809
12	99TM–23	"AT, lower"		SQPBHCSpZMI	77.5	0.150	11.6	1.03	0.06	0.40	0.60	2.80	4.29	0.05	0.02	1.75	100.3	196	62	40	33	142	162	3.2	803
13	99TM–17	"AT, upper"	19	PSQBHCSpZMI	73.1	0.247	13.4	1.48	0.08	0.21	0.76	3.97	4.80	0.03	0.02	2.05	100.1	162	75	37	30	374	293	2.2	842
14	99TM–22	"AT, upper"	22	PSQBHCSpZMI	72.7	0.308	14.2	1.65	0.08	0.30	0.61	3.61	5.54	0.03	<0.01	1.10	100.1	192	104	35	29	654	379	1.8	874
15	RW18B3–4‡	"AT, upper"	17	PSBMCIZ	61.4	0.721	17.4	3.68	0.11	1.02	2.52	4.67	5.47	0.20	ND	2.65	99.8	101	750	ND	ND	4429	1548	0.1	1014
16	85FB61-A‡	"AT, upper"	16	PSBHCSpZMI	59.4	1.143	15.8	4.30	0.13	1.90	2.31	3.98	5.53	0.26	ND	ND	94.8	102	730	ND	ND	5148	1843	0.1	1014
17	99TM–21	post-AT	20	PSQBHCSpZMI	74.0	0.169	11.3	1.17	0.09	0.67	2.4	1.68	2.92	0.03	0.01	5.75	100.2	136	235	46	28	173	153	0.6	795

Note: Coordinates (UTM): Yucca Mt west slope: (1) 0546956/4076224; (2) 100 m up of the previous location; (3) 0547211/4076210; (4) 0546448/4077988; Nevada Test Site: (5) 0562016/4120554; (6) 100 m east of the previous location; (7) 0553924/4125594; (8) 0549590/4116290; (9) ???; (10) Old Pahute Mesa Rd; (11) 0555203/4124672; (12) 0549617/4115983; (13) 0565336/4111835; (14) 0555674/4101452; (15) ND; (16) ND; (17) 0565336/4111835.

†Q—quartz, S—Sanidine, P—plagioclase, B—biotite, H—hornblende, C—clinopyroxene, Sp—sphene, M—magnetite, I—ilmenite, Z—zircon; Q,S,P,and B are given in decreasing order of abundance.

‡Samples of R.G. Warren (Warren et al., 1989; 1998).

§T Zrc sat—temperature of zircon saturation based on Watson and Harrison (1983).

ND—no data.

matic modification of $\delta^{18}O$(whole rock). The preservation of primary magmatic $\delta^{18}O$ values in rocks is supported if there are small and consistent fractionations of $\delta^{18}O$ between minerals. In contrast, hydrothermally altered rocks show wide variations in $\delta^{18}O$ values and irregular mineral to mineral fractionations. In this work, we make a clear distinction between magmatic oxygen isotope ratios, $\delta^{18}O$(magma), calculated from the composition of unaltered and refractory phenocrysts, and measured whole-rock values; the latter are relevant only for study of secondary alteration. In particular, many whole-rock analyses of TS and TC tuffs reported high $\delta^{18}O$ (>+10‰: Neymark et al., 1995; Marshall et al., 1996), and we demonstrate in this paper that $\delta^{18}O$ (whole rock) values result from low-temperature (<100 °C) exchange of volcanic glass with surface waters.

The practical goal of our study involves the fact that the proposed high-level nuclear waste repository at Yucca Mountain is in Topopah Spring and Tiva Canyon tuffs. There is an ongoing discussion of pedogenic versus hydrothermal origins of carbonate cements and mineralization in faults that cross-cut Yucca Mountain, which are relevant to the safety of the repository (Rumble, 1992; U.S. Department of Energy, 1993; Chepizhko et al., 1996; Dublyansky et al., 1998, 2001). Oxygen isotope studies provide central evidence in any model involving circulation of hydrothermal fluids. Understanding the extent, age, and mechanisms of hydrothermal activity should be based on accurate estimation of the $\delta^{18}O$ of primary source rocks and the mechanisms of water-rock interaction. Therefore, the practical objective is to measure $\delta^{18}O$ values of phenocrysts in order to determine the primary value of $\delta^{18}O$ in tuffs. We show that zircon, sphene, and other minerals in carbonate cements of Yucca Mountain did not precipitate from hydrothermal solutions, and were mechanically extracted from tuffs during fault movements (Bindeman and Valley, 2000; Appendix 2, Data Repository).[1]

Sample Collection and Analytical Techniques

Samples (individual pumice clasts and densely welded tuff portions) were collected using published maps (Byers et al., 1976a, 1976b; Frizzell and Shulters, 1990; Day et al.,

[1]GSA Data Repository item 2003066, Minerals in carbonate cement of Yucca Mountain, is available on the Web at http://www.geosociety.org/pubs/ft2003.htm. Requests may also be sent to editing@geosociety.org.

1999), and a global positioning system (GPS) (Table 1). Thin sections were made from each rock and optically examined for mineralogy, texture, crystal content, and degree of alteration. Individual phenocrysts of quartz and sanidine were selected from hand specimen or from crushed rock. Quartz was treated with cold fluoroboric acid to remove adhered feldspars and glass. Zircons were separated from ~20 kg rock samples using standard techniques of crushing and density separation and then purified with cold HF and HNO_3. Separates of 50–250 mg of zircon were further subdivided by sieving into different sizes. Magnetite and ilmenite crystals were removed from crushed rock by using a strong ceramic magnet. Ilmenite was then concentrated in a mixture by using a weak magnet to remove magnetite.

Air abrasion in a corundum mortar allowed us to retrieve and analyze cores of quartz, magnetite, sphene, and zircon crystals. Air abrasion of magnetite also helped to remove surface oxidation and alteration. Weighing of the starting and remaining material provides an estimate of the decrease in the average radius. Air abrasion of larger-diameter zircons (>105 μm or >149 μm) took from 0.5–5 days.

The University of Wisconsin–Madison CO_2 laser fluorination/mass-spectrometer system (Valley et al., 1995) provides rapid and precise determination of $\delta^{18}O$ for silicate and oxide minerals. Samples were typically 1–2 mg, yielding 10–30 μmols of CO_2. BrF_5 was used as a reagent. Quartz phenocrysts were analyzed by rapid heating, mostly as single grains, yielding particularly precise values (better than ±0.1‰, 1 standard deviation; Spicuzza et al., 1998a). For analyses of more reactive sanidine and glass, an airlock sample chamber was used to prevent partial prereaction (Spicuzza et al., 1998b). From 4 to 7 aliquots of UWG-2 garnet standard were measured at the beginning and end of each analytical session, and sample data were adjusted according to the average value of the standards, typically by <0.12‰. The average reproducibility of 65 UWG-2 analyses is 0.10‰ (1 standard deviation). NBS-28 quartz analyses yielded an average value of 9.45‰ (±0.11‰, 1 standard deviation n = 19, V-SMOW).

Chemical analyses were by X-ray fluorescence spectrometry (XRF) or electron microprobe (EMPA). Whole-rock chemical analyses for major and trace elements (Rb, Ba, Sr, Y, Nb, Zr) were made at XRAL Laboratories (Ontario, Canada) by XRF. The uncertainty of trace element determinations is ±2 ppm. Ten polished magnetite and ilmenite grain mounts were imaged with backscattered electrons to determine degree of exsolution, Least exsolved grains were analyzed (1300 analyses) by wavelength dispersive analysis for major and minor elements on a Cameca SX-50 electron microprobe at the University of Wisconsin-Madison using 15 kV accelerating voltage and 25 nA sample current with minerals as standards.

RESULTS

Petrography of Analyzed Samples

Each tuff unit exhibits gradational transitions in phenocryst content, mineralogy, and chemical composition (Table 1, see also Schuraytz et al., 1989; Flood et al., 1989; and Mills et al., 1997 for detailed description of chemical analyses of SWNVF). Rhyolitic portions of each tuff unit, as well as pre-AT rhyolite lava are crystal poor (2%–16% phenocrysts). They contain phenocrysts of (in decreasing order): sanidine, plagioclase, quartz, biotite, hornblende, clinopyroxene, and magnetite. Accessory minerals are represented by large (0.5–1 mm), scarce euhedral sphene, scarce ilmenite, zircon, and apatite. Ilmenite was not found in TC.

Latitic portions of each tuff and post-AT lava contain 17%–35% phenocrysts (in decreasing order): plagioclase, sanidine, biotite, clinopyroxene, hornblende, and magnetite. Feldspars and biotite are abundant in latites, while quartz is either rare (in RM and AT tuffs) or absent (in TC and TS tuffs). Among accessory minerals, sphene is rare (absent in TS tuff), often resorbed; however, ilmenite, zircon, and apatite are more abundant than in rhyolites. Warren et al. (1989) note the occasional presence of orthopyroxene, perrierite, and allanite in latites of RM, and scarce monazite in all other tuff units. It is noteworthy that there is an anticorrelation in the abundance of sphene and zircon: samples of high-silica rhyolites that have large (0.3–1 mm) euhedral sphene contain very little zircon (and low zirconium), while samples of latites that have small (<0.2 mm) resorbed sphene contain abundant zircon. Phenocrysts in rhyolites are euhedral to subhedral, while in latites they are more fragmented and resorbed. Optically, plagioclase phenocrysts exhibit higher anorthite content ($An_{55–25}$), and complex (normal and reverse) zoning within single crystals. Latites and rhyolites have a distinct composition of minerals and distinct composition of glass (Warren et al., 1989; Mills et al., 1997).

Whole-rock major and trace element concentrations and ratios exhibit wide gradational variations within each tuff (Table 1), discussed by Lipman et al. (1966), Byers et al. (1976a), Broxton et al. (1989), and Mills et al. (1997). For example, the Rb/Sr ratio reaches 20 for most differentiated pre-AT high-silica rhyolites, but is 0.5–5 for most rocks and there is an anticorrelation of the Rb/Sr ratio and MgO (Fig. 2). Both whole-rock and sanidine analyses show that the latitic portions contain twice the amount of Nd and three to four times more Sr than do rhyolitic portions (Farmer et al., 1991; present study, Table 1). High values of Rb/Sr in some rhyolites suggest that rhyolites could be much more susceptible to contamination by high $^{87}Sr/^{86}Sr$

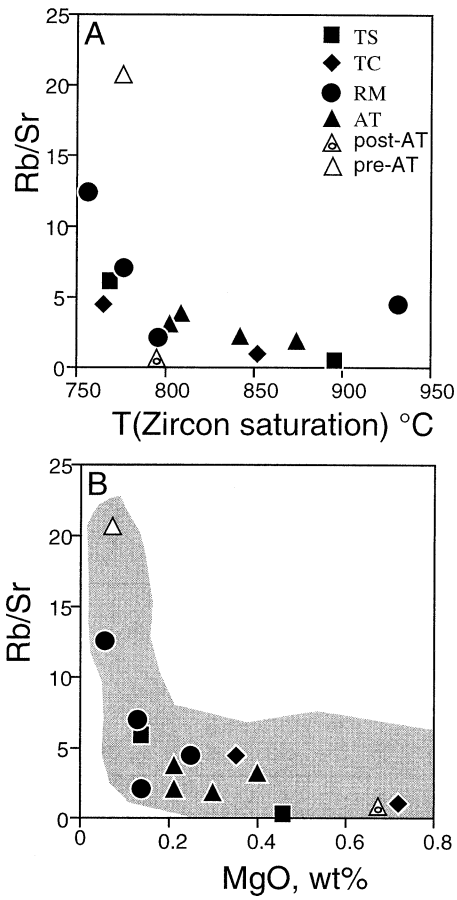

Figure 2. Compositional trends in studied samples from Timber Mountain/Oasis Valley Caldera Complex (see Table 1 for analyses). (A) Zircon saturation temperature, calculated using Watson and Harrison (1983) vs. Rb/Sr ratio. Notice that most differentiated (high Rb/Sr) samples are Zr-poor and have lower zircon saturation temperatures. (B) Rb/Sr ratio vs MgO. Shaded field is other published data for SWNVF (see text).

country rocks than are latites. Importantly, there is no correlation between chemical parameters and $\delta^{18}O$(melt) values (see below), and we found no trace elements or ratios to fingerprint low-$\delta^{18}O$ magmas of the AT cycle.

The concentration of Zr changes from <100 ppm in some high-silica rhyolites to 800 ppm in some latites, and calculated zircon saturation temperatures (Table 1) are 750–950 °C (Fig. 2). Similarly, temperature estimates based on magnetite-ilmenite cation thermometry (Appendix 1) differ from 50 °C to >150 °C between latites (850–950 °C) and rhyolites (700–750 °C). Lipman (1971), Schuraytz et al. (1989), and Mills et al. (1997) noticed a reverse correlation between SiO_2 content of the whole rock and the temperature estimated using Fe-Ti oxides in TS, AT and RM, and TC tuff units, respectively. Such a relationship suggests that silicic portions located near the top of the magma chamber were ~150–200 °C colder, signifying a steep thermal gradient in preclimactic magma chambers.

Oxygen Isotope Composition of Phenocrysts

Individual phenocrysts of quartz, sanidine, and bulk samples of magnetite, zircon, and sphene (size fractions and air-abraded cores) were analyzed (Table 2). The $\delta^{18}O$ values are plotted versus $^{40}Ar/^{39}Ar$ age or stratigraphic sequence of eruption (Fig. 3). Analyses of phenocrysts show small $\Delta^{18}O$(mineral-mineral) fractionations consistent with eruptively quenched magmatic temperatures (700–900 °C) when experimental oxygen isotope thermometers (e.g., Chiba et al., 1989) are applied. Latitic portions of each tuff are characterized by smaller $\Delta^{18}O$(mineral-mineral) values than those in colder rhyolitic portions. For magnetite (Mt), $\Delta^{18}O$(mineral-Mt) reaches 4–6‰, and Δ(quartz-Mt) and Δ(Sanidine-Mt) provide the maximum resolution and were used to calculate oxygen isotope temperatures (Table 2, Appendix 1). Air-abraded cores of magnetites were analyzed and yielded a magmatic temperature range of 700–800 °C for rhyolites, and 800 °C to >900 °C for latites. Temperatures based on Fe-Ti oxides give similar, but systematically lower, range (Fig. A1).

The $\delta^{18}O$ values in each mineral (Fig. 3) vary distinctly in each tuff unit: all minerals in the TC tuff are 1.5‰ lower than in the TS tuff, and the AT tuff is 2.5‰ lower than the preceding RM tuff. There is no significant difference in $\delta^{18}O$ values between individual phenocrysts of quartz and the bulk of quartz, suggesting little $\delta^{18}O$ variability among different crystals within any given sample of

TABLE 2. OXYGEN ISOTOPE COMPOSITION AND CALCULATED TEMPERATURES OF MAJOR TUFFS AND LAVAS OF TIMBER MOUNTAIN/OASIS VALLEY CALDERA COMPLEX, SOUTHWEST NEVADA VOLCANIC FIELD

Sample Mineral	$\delta^{18}O$	$\Delta^{18}O$, T Qz-Mt (°C)	San-Mt (°C)	T Mt-Ilm (°C)	log(fO_2) bars	$\delta^{18}O$ melt (‰)	$\Delta^{18}O$ melt-min	ϵNd	$^{87}Sr/^{86}Sr_i$
99TM–11, TS, rhyolite									
San	8.37		795	748	−15.7	8.68	0.31	−11.5	0.712
Sph, xenocryst	7.07						1.61	−11.7	
Zrc, blk	7.05						1.63		
Zrc, blk	6.88						1.80		
Mt	3.68						5.00		
99TM–10, TS, latite									
Qz-1, m	8.93	872	965	978	−9.7	8.06	−0.87	−10.6	0.715
San, 2xtls	7.62						0.44	−11.1	
Zrc, blk	6.76						1.30		
Zrc, blk	6.84						1.22		
Zr, <53	6.64						1.42		
Zr, <53	6.50						1.56		
Zr, >149	6.61						1.45		
Mt	4.09						3.97		
Mt	4.17						3.89		
99TM–7, TC, rhyolite									
San-1	6.91		788			7.42	0.51	−11.16	0.711
Sph	4.74						2.68		
Zrc, blk	5.90						1.52		
Mt	2.16						5.26		
Cpx	5.59						1.83		
Amph	5.06						2.36		
99TM–12, TC, latite									
San-1	6.84		970	838	−12.3	7.25	0.41	−10.77	0.7088
San	7.20						0.05		
Sph	4.76						2.49		
Zrc, <53	5.68						1.57		
Zrc, bulk	5.93						1.32		
Zrc, >149, 60%	5.88						1.37		
Mt	3.56						3.69		
99TM–13, RM, rhyolite									
Qz, b	9.10	747	759	671	−16.0	8.30	−0.80	−11.27	0.713
Qz, b	8.94						−0.64		
San	8.00						0.30		
Zrc, blk	6.54						1.76		
Zrc, blk	6.61						1.69		
Mt	2.93						5.37		
Mt	3.03						5.27		
Cpx	5.65						2.65		
99TM–14, RM, rhyolite									
Qz, m	8.84	577				8.11	−0.73	−11.27	0.713
Qz, b	8.86						−0.75		
Qz, b	8.88						−0.77		
Qz, s	8.89						−0.78		
Mt	0.15						7.96		
99TM–16, RM, rhyolite									
Qz, m	8.40	748	711	718	−15.1	8.13	−0.27	−10.45	0.70843
Qz, s	8.64						−0.51		
Qz, b	8.58						−0.45		
San	8.03						0.10		
Sph	5.91						2.22		
Zrc, blk	6.43						1.70		
Zrc, blk	6.60						1.53		
Zrc, >105	6.47						1.66		
Zrc, <53	6.48						1.65		
Mt	2.50						5.63		
Mt	2.50						5.63		
99TM–26, RM, latite									
Qz, b	8.07					7.39	−0.68	−10.45	0.70843
FB18el–3, RM, latite									
Qz-1	7.56	917	900			7.51	−0.05	−10.45	0.70843
Qz-1, xenocryst	9.03						−1.52		
San-1	6.99						0.52		
San-1	7.33						0.18		
San-1	7.06						0.45		
Mt	3.12						4.39		
Mt	3.08						4.43		

each tuff unit (Table 2, Fig. 3). In particular, 50% air-abraded cores of individual quartz phenocrysts, and air-abraded cores in sphene phenocrysts in all samples (including low-$\delta^{18}O$ rocks of AT cycle), are undistinguishable from $\delta^{18}O$ of smaller crystals of quartz and sphene (Table 2). This result contrasts SWNVF to Yellowstone where low-$\delta^{18}O$ lavas show 2‰ variability among individual quartz crystals (Bindeman and Valley, 2001). Only zircon in AT tuff, post-AT lava, and pre-AT lava preserves oxygen isotope zoning (see below).

The Calculated $\delta^{18}O$ Values of Melt

In this paper, values of $\delta^{18}O$(melt) are calculated from measured $\delta^{18}O$ values of pristine phenocrysts and the estimated magmatic temperature. We use analyses of quartz, sanidine, sphene, and zircon (except in AT tuff where zircon is zoned), and temperature estimates based on quartz-magnetite and sanidine-magnetite oxygen isotope thermometry (Table 2). Experimental and empirical $\Delta^{18}O$ (mineral-melt) fractionations were employed (Fig. 4) to derive $\delta^{18}O$(melt) values. Each mineral in a sample yielded a single $\delta^{18}O$(melt) value, and different minerals in a sample yielded a narrow range (typically <0.3‰) of calculated $\delta^{18}O$(melt) values (Fig. 5). This range could result from uncertainty of employed fractionations and analytical uncertainty of each analysis. The average composition of $\delta^{18}O$(melt) was calculated for each sample and is shown on Figure 3. Glass compositions in latites and rhyolites of SWNVF are low-silica rhyolitic (LSR), and high-silica rhyolitic (HSR), respectively (Mills et al., 1997). We calculated normative CIPW compositions of glass and assumed that $\Delta^{18}O$(quartz-HSR) and $\Delta^{18}O$(quartz-LSR) fractionations will vary linearly with proportions of normative albite, orthoclase, and quartz components. The resulting $\Delta^{18}O$(quartz-HSR) is ~0.2‰ smaller than $\Delta^{18}O$(quartz-LSR).

The $\delta^{18}O$(magma) value (magma = melt + crystals) can be calculated as a linear combination of $\delta^{18}O$(melt) and $\delta^{18}O$(phenocrysts), proportions of melt, and proportions of different phenocrysts for each sample. In crystal-poor (1%–15%) rhyolites, the majority of phenocrysts is represented by quartz and feldspar, and their addition to the melt has a small, subpermil effect on the resulting $\delta^{18}O$(magma). Because $\Delta^{18}O$(quartz-melt) and $\Delta^{18}O$(feldspar-melt) have opposite signs (see Fig. 4), addition of equal amounts of these phenocrysts has almost no effect on $\delta^{18}O$(magma). Thus, the calculated $\delta^{18}O$(melt) is equal to

TABLE 2. (*Continued*)

Sample Mineral	$\delta^{18}O$	$\Delta^{18}O$, T Qz-Mt (°C)	San-Mt (°C)	T Mt-Ilm (°C)	log(fO_2) bars	$\delta^{18}O$ melt (‰)	$\Delta^{18}O$ melt-min	ϵNd	$^{87}Sr/^{86}Sr_i$
99TM–15, AT, rhyolite									
Qz, b	6.31	762	766	662	−16.6	5.57	−0.74	−10.3	0.715
Qz, b	6.25						−0.68		
Qz, 12% abr	6.22						−0.65		
Qz, 40% abr	6.14						−0.57		
San-1	5.32						0.25		
Zrc, <53	4.26						1.31		
Zrc, 53<x<105	4.37						1.20		
Zrc>105	4.53						1.04		
Zrc>105, 25% abr	4.61						0.96		
Sph, >0.5 mm, 55%	2.71						2.86		
Sph, <0.25 mm	2.73						2.84		
Sph	2.67						2.90		
Mt	0.19						5.38		
Mt	0.79						4.78		
Mt	0.10						5.47		
99TM–23, AT, rhyolite									
Qz, b	6.18					5.48	−0.70	−10.3	0.715
Qz, b	6.31						−0.83		
Qz, s	6.24						−0.76		
99TM–17, AT, low-silica rhyolite									
Qz, m	5.79	870	899	816	−12.3	5.39	−0.40	−9.45	0.7078
Qz, b	5.86						−0.47		
Qz, m	6.15						−0.76		
Qz, b	6.43						−1.04		
San-1	5.13						0.26		
Zrc, <53	4.37						1.02		
Zrc, <105, >53	4.28						1.11		
Zrc, >105	4.59						0.80		
Zrc, >105	4.55						0.84		
Zrc, >105, 30%	4.63						0.76		
Zrc, >105, 40%	4.59						0.80		
Zrc, >105, 40%	4.76						0.63		
Sph, <0.25 mm	2.82						2.57		
Sph, >0.5mm, 33%	2.68						2.71		
Mt, b	0.93						4.46		
Mt, s	1.38						4.01		
Mt	1.42						3.97		
99TM–22, AT, latite									
Qz, b	6.22					5.48	−0.74	−9.45	0.7078
Qz, b	6.11						−0.63		
85FB61-A, AT, latite									
San-1	5.88		946			6.18	0.28	−9.45	0.7078
Mt	2.34						3.82		
Mt	2.23						3.93		
RW18B3–4, AT, latite									
Qz-1	6.25	958	981			5.88	−0.37	−9.45	0.7078
Qz-1	6.51						−0.63		
San-1	5.74						0.14		
San	5.57						0.31		
San-1	5.58						0.30		
Mt	2.23						3.65		
Mt	2.24						3.64		
99TM–21, post-AT, rhyolite									
Qz, m	6.00	784				5.45	−0.55	−9.64	0.70776
Qz, b	6.50						−1.05		
Qz, b	6.12						−0.67		
Qz-1, 60%	6.59						−1.14		
Zrc, <53 um	4.14						1.31		
Zrc, bulk, 10%	4.60						0.85		
Mt	0.72						4.73		
Mt	0.63						4.82		
99TM–24, pre-AT, rhyolite									
Qz, m	6.36	754	744	710	−14.8	5.73	−0.63		0.71358
Qz, m	6.37						−0.64		
Qz, b	6.15						−0.42		
Qz, b	6.40						−0.67		
Qz, s	6.34						−0.61		
San	5.53						0.20		
Sph, bulk	3.60						2.13		
Sph, <0.25 mm	3.16						2.57		

TABLE 2. (*Continued*)

Sample Mineral	$\delta^{18}O$	Δ18O, T Qz-Mt (°C)	San-Mt (°C)	T Mt-Ilm (°C)	log(fO_2) bars	$\delta^{18}O$ melt (‰)	$\Delta^{18}O$ melt-min	εNd	$^{87}Sr/^{86}Sr_i$
Sph, >0.5 mm, 44%	3.52						2.21		
Sph, >0.25	3.03						2.70		
Zrc, 53<x<105	4.49						1.24		
Zrc, blk	4.38						1.35		
Zrc, blk	4.47						1.26		
Zr, >105, 50%	4.83						0.90		
Mt	0.36						5.37		
99TM–29, Carbonate cement of Trench 14, Yucca Mountain									
Sphene	4.03	744	734	Inside sphene xtls					
Sphene	3.88			899	−11.3				
Mt	2.62			and					
Brown glass	8.03			786	−12.8				
Fsp, 1 ind	7.90								
Green Cpx, many	5.65								
Black Hb, many	5.00								
Zrc, bulk	6.35								
Qz, 4 xtls	9.44								

Note: Major and trace element analyses are given in Table 1. $\delta^{18}O$(magma) is calculated assuming the fractionation factors and temperature (see Fig. 4 and text for discussion). Sr and Nd isotopic values for the same units are from Farmer et al. (1991) and Noble and Hedge (1969). <53, >105, >149 (μm) are zircon size fractions (diameter); 40% is 40 vol. % abraded cores (60% remaining); s, m, b are small, medium, big crystals in each rock; Qz-1 is an individual quarz phenocryst; blk—bulk analysis; xtls—crystals; Qz—quartz; Zrc—zircon; San—sanidine; Mt—magnetite; Sph—sphene; Cpx—clinoproxene; Hb—hornblende.

$\delta^{18}O$(magma) within uncertainty of ±0.05‰. In more crystal-rich (15%–30%) latites, high $\delta^{18}O$ mineral quartz is less abundant or absent, and the majority of phenocrysts (10%–25%) are represented by slightly lower $\delta^{18}O$ feldspars and strongly lower $\delta^{18}O$ Fe-Mg minerals (biotite+ clinopyroxene + hornblende, 1%–5%). We estimate that the combined effect of addition of these minerals should lead to 0.1‰ to a max 0.3‰ lower $\delta^{18}O$(magma) value than $\delta^{18}O$(melt). Keeping this in mind, we choose to plot and discuss $\delta^{18}O$(melt) values of latites for the purpose of comparison with $\delta^{18}O$(melt) values of rhyolites (Fig. 3).

The calculated values of $\delta^{18}O$(melt) in four major tuffs of SWNVF are distinctly different for each tuff (Fig. 3) and are significantly lower than $\delta^{18}O$ values based on whole rock analyses ($\delta^{18}O$ = 9–16‰, Neymark et al., 1995; Marshall et al., 1996). We conclude that these reported high-$\delta^{18}O$(whole rock) values result from low-temperature secondary alteration of volcanic glass by meteoric waters and are not useful in understanding the $\delta^{18}O$ values of magma.

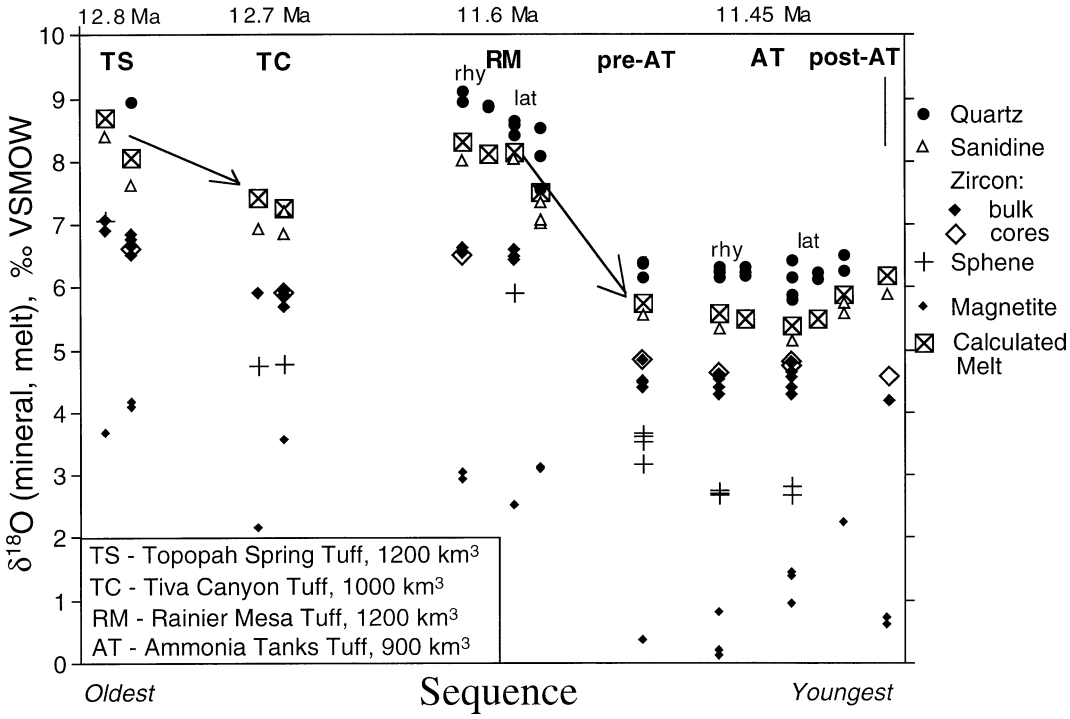

Figure 3. Evolution of $\delta^{18}O$ in minerals (measured) and melt (calculated, see text and Fig. 4) of four major tuffs and two lavas from SWNVF (data are from Table 2). Notice sudden depletion of $\delta^{18}O$ after TS and RM. AT represents low-$\delta^{18}O$ magma. First column(s) of each unit is rhyolite, second is latite; there are two samples of latite and rhyolite in RM, and two samples of rhyolite and three samples of latite in AT. Notice smaller mineral-mineral isotopic fractionation in latites as compared to rhyolites due to higher temperature of the former. Notice that air-abraded cores of zircons are higher in $\delta^{18}O$ than are bulk zircons or smaller zircons in AT tuffs, pre-AT lave, and post-AT lava.

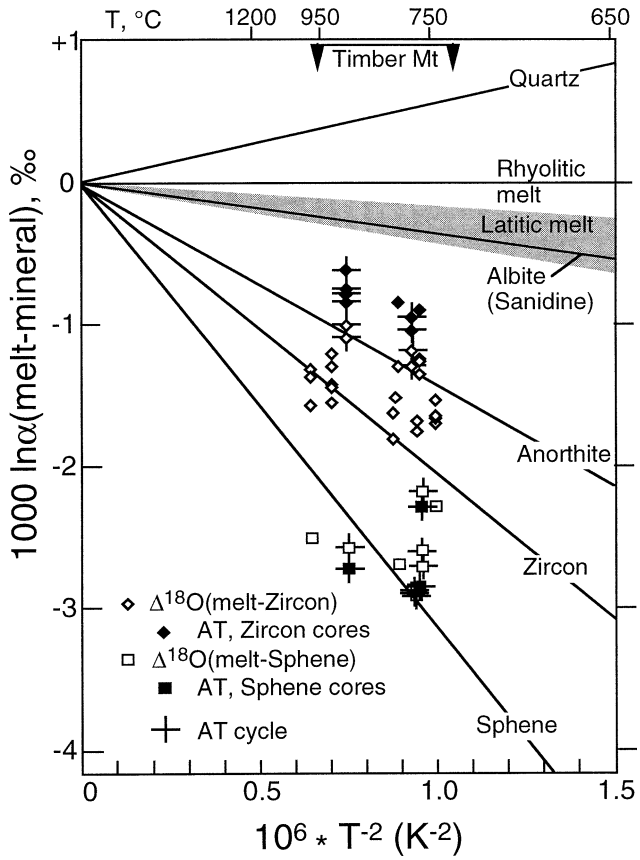

Figure 4. Experimental and empirical mineral-melt fractionations used in the present study to calculate $\delta^{18}O$(melt) based on $\delta^{18}O$(mineral) and temperature. Anorthite-, albite-, and quartz-rhyolite fractionations are calculated using experiments (Palin et al., 1996; Matthews et al., 1994, 1998; Stolper and Epstein, 1991). Zircon-rhyolite, and sphene-rhyolite fractionations are calculated using experimental quartz-rhyolite and the empirical quartz-zircon and quartz-sphene fractionations (Valley et al., 2003; King et al., 2001). Rhyolite-latite isotopic fractionation is shown in shaded field assuming that latite melt is a mixture of rhyolite and normative feldspars (albite and sanidine). Data points are zircon-melt and sphene-melt fractionations for SWNVF at calculated $\delta^{18}O$(melt) and temperatures from Table 2 and intend to show: 1) smaller than equilibrium values $\Delta^{18}O$(melt-zircon) for AT cycle magmas, especially for zircon cores; 2) lack of such systematic distinction for sphene; and 3) overall equilibrium fractionations (with scatter) for zircon and sphene in other magmas of SWNVF.

The reconstructed value ranges of $\delta^{18}O$(melt) in rhyolitic and latitic portions of each tuff and intracaldera lavas are plotted versus published $^{87}Sr/^{86}Sr_i$ and ε_{Nd} isotope values for the same units (Fig. 5). Noble and Hedge (1969) and Farmer et al. (1991) noticed that the initial $^{87}Sr/^{86}Sr$ ratios of sanidines of rhyolitic portions of each tuff are significantly higher than that of the latitic portion. Farmer et al. (1991) discovered that rhyolites also have lower whole-rock ε_{Nd}. We note that: 1) each unit is characterized by a distinct range of $\delta^{18}O$(melt) values; 2) rhyolites are 0.5–1‰ higher in $\delta^{18}O$(melt) than latites of the same tuff, except in AT where there is <0.2‰ difference; 3) each tuff has a unique zoning pattern: negative correlation of $\delta^{18}O$(magma) versus $^{87}Sr/^{86}Sr_i$ for TS tuff; positive for RM and TC tuffs; and no correlation for AT tuff; 4) rocks of the AT cycle were low-$\delta^{18}O$ magmas and have the least negative ε_{Nd} (Fig. 5; Farmer et al., 1991) of all SWNVF volcanic rocks.

Oxygen Isotope Zoning in Zircons

We performed analyses of several zircon size fractions from each tuff: bulk, smaller-size fractions (<53 μm in diameter), larger-size fractions (>105 μm, >149 μm), and air-abraded cores. Rhyolitic and latitic portions of TS, TC, and RM tuffs exhibit no difference between large and small zircons or zircon cores retrieved by air abrasion (Table 2). The $\delta^{18}O$ values of zircon are in equilibrium with other minerals for all tuff units (except low-$\delta^{18}O$ rocks of the AT cycle): pre-AT rhyolitic lava, rhyolitic and latitic portions of AT tuff, and post-AT crystal-rich latitic lava (Table 2). In these samples, air-abraded cores of larger (>105 μm) zircons are 0.4–0.5‰ higher in $\delta^{18}O$ than of smaller (<53 μm) zircons (Table 2). Such differences exceed analytical uncertainty (±2 standard deviation, less than ±0.2‰) and suggest 1.5–2‰ $\delta^{18}O$ zoning in zircon crystals in low-$\delta^{18}O$ AT tuffs when compared to the curves based on successive air-abrasions of >105 μm zircons (Fig. 6). Additionally, $\Delta^{18}O$(quartz-zircon) for these samples is 1.6–1.8‰, while $\Delta^{18}O$(melt-zircon cores) is 0.6–0.9‰ (Fig. 4), which is 0.5–0.9‰ smaller than equilibrium values at 750–850 °C in similar rhyolites of Bishop Tuff (Bindeman and Valley, 2002). Even smaller (<53 μm) zircons show somewhat lower $\Delta^{18}O$(quartz-zircon) and $\Delta^{18}O$(melt-zircon) fractionations, although closer to equilibrium. The quartz-zircon and melt-zircon disequilibria are a direct result of zircon zoning due to elevated values of $\delta^{18}O$(zircon) cores, since quartz is in equilibrium with melt and other minerals (Table 2). The discovery of oxygen isotope zoning in zircons in low-$\delta^{18}O$ tuff and lavas of SWNVF is a significant result, which is similar to oxygen isotope zoning in zircons in low-$\delta^{18}O$ lavas of Yellowstone (Bindeman and Valley, 2001).

The lack of zoning in sphene is unlikely to be due to diffusion. On the time scale of oxygen exchange between small zircons and melt, the 5–10 times larger in length crystals of sphene should preserve zoning, even though "wet" diffusion in sphene is 10–15 times faster (Morishita et al., 1996), unless diffusion coefficients of oxygen are significantly faster than current estimates (e.g., Zhang et al., 2001). More likely, if sphene were inherited from a higher-$\delta^{18}O$ source, it was recrystallized as is evident by the surface resorption features for sphene in latites. Additionally, recrystallization is more likely for sphene than for zircon because sphene is made of major elements of the melt (Ca, Ti, Si) and is stable in the narrower field of P-T-f_{O2} (Xirouchakis and Lindsley, 1998). Zircon is made of a slow diffusing trace element Zr and is stable in a much wider range of temperatures and compositions (e.g., Watson and Harrison, 1983).

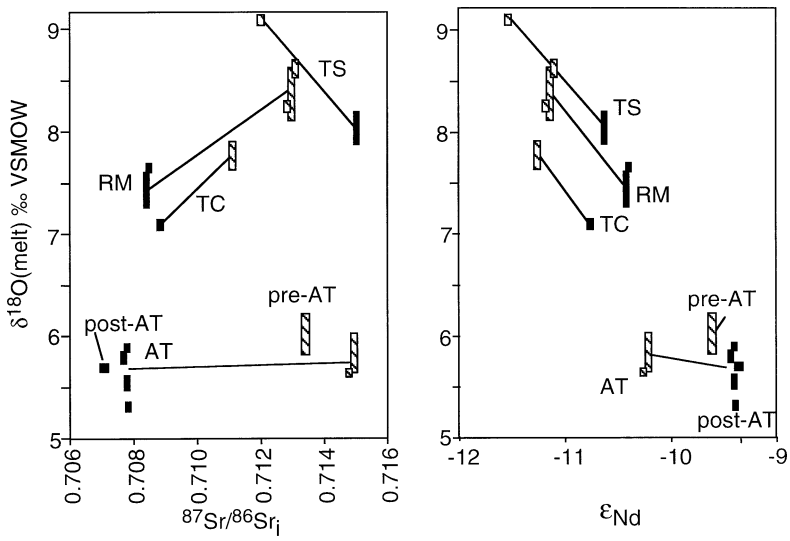

Figure 5. Values of $\delta^{18}O$(melt) vs. initial (at the time of eruption) $^{87}Sr/^{86}Sr_i$ and ε_{Nd} (from Farmer et al., 1991) for rhyolitic and latitic samples. Open pattern denotes rhyolitic portion of each tuff; dark pattern is used for upper, latitic portions. Tie-line connects early and late units from a single tuff. Notice internal zoning of each tuff with respect to all three isotopic ratios. Ammonia Tanks tuff is weakly zoned with respect to $\delta^{18}O$, and its latitic and rhyolitic portions are similarly $^{18}O/^{16}O$ depleted as are pre-AT and post-AT lavas. All these units of AT-cycle contain zircons that are zoned in $\delta^{18}O$ (Fig. 6). Compositional zoning in magmas of AT-cycle is much more complex than in the other tuffs, and this has been attributed to caldera collapse/vent dynamics (Christiansen et al., 1977) and/or multiple magma types (Mills et al., 1997).

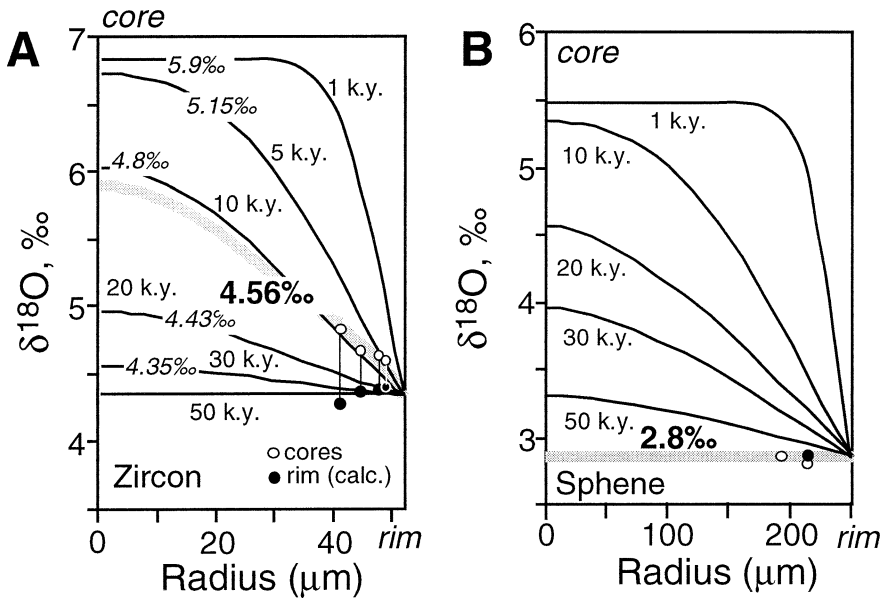

Figure 6. Oxygen isotope zoning profile through zircons (A) in Ammonia Tanks tuff, and the calculated equilibration time using diffusion coefficient for water-saturated oxygen diffusion at 850 °C (from Watson and Cherniak, 1997), solved numerically for diffusion in a sphere using Crank (1975); see Bindeman and Valley (2001) for details. Sphene equilibration curves (B) were calculated using diffusion coefficients from Morishita et al. (1996) and the same procedures. Note that preservation of oxygen isotope zoning in sphene is as expected given large size (0.5 mm) of sphene crystals if sphene were inherited from normal-$\delta^{18}O$ rocks; see text for discussion.

DISCUSSION

Oxygen Isotope Constraints on the Independent Nature of Each Eruptive Unit

Several researchers have suggested that the different tuff units could be related to a long-lived, batholith-scale, differentiating magma body (Broxton et al., 1989). We described that all four tuff units have distinct values of $\delta^{18}O$(magma), corroborating differences in Sr and Nd isotopes and chemistry (Fig. 5). However, oxygen is a major element in magmas and rocks, and oxygen isotopic differences between TS and TC, and RM and AT tuffs cannot be explained by assimilation based on mass and heat balance constraints. For example, if the $\delta^{18}O$ of bulk assimilant is low (e.g., 0‰), then the $\delta^{18}O$(melt) requires 20% of assimilant to generate TC from TS and 35% to produce AT by adding assimilant to RM magma. If assimilant is assumed to have a more realistic, higher $\delta^{18}O$, then even higher amounts of assimilant would be necessary. Following on with the famous Bowen argument, rhyolitic and latitic magmas do not have enough superheat to experience such a great degree of bulk transformation. If a high percentage of assimilation had occurred, the resultant assimilating silicic magma would become exceedingly crystal rich. This is not observed; all tuffs at SWNVF are crystal poor. Therefore, the isotopic differences between tuffs strongly suggest that each voluminous tuff unit is a result of eruption of an independent, internally zoned magma body that cannot be derived by fractionation and assimilation from magma of the previous cycle. A number of researchers have presented chemical evidence for an independent nature of each tuff unit at SWNVF. Lipman (1966) and Schuraytz et al. (1989) concluded that TC represents a different magma batch than TS, based on major and trace elemental chemical differences. Mills et al. (1997) and Huysken et al. (1994) reached similar conclusion for RM and AT tuffs on the basis of differing chemistry of minerals and glass.

Proposed here is a new portion of hot mafic magma with mantle-like $\delta^{18}O$ that initiated the generation of low-$\delta^{18}O$ or high-$\delta^{18}O$ silicic magmas by melting of low-$\delta^{18}O$ or high-$\delta^{18}O$ rocks in an extensional tectonic environment. The presence of mafic pumice (52%–57% SiO_2) among late-erupted portions of each tuff (Warren et al., 1989; Table 1) supports the hypothesis that fresh basaltic magma initiated each cycle in which eruptive draw-down was deep enough to tap the bottom parts of each magma chamber, and that caldera collapse

evacuated most silicic differentiated products in the magma chamber. This activity could have been accomplished if the magma bodies were shallow, sheet-like intrusions because such shape would enhance the efficacy of magma chamber evacuation during eruption and promote rapid cooling and fractionation on a short (100 k.y.) time scale (e.g., Huppert and Sparks, 1988). Given the caldera areas of 400–800 km^2 (Fig. 1) and eruptive volumes of 900–1200 km^3, the thickness of such a magma chamber, equal to eruptive drawdown, is expected to be from 1 to 2.5 km. In contrast, other large silicic magma systems like Bishop Tuff are long-lived ($\sim 10^6$ yr), are at least 4–5 km thick, and have homogeneous $\delta^{18}O$(melt) values (e.g., Bindeman and Valley, 2002). The generation of successive and relatively short-lived, sheet-like magma bodies in SWNVF are possibly related to a specific extensional tectonic environment in this part of the Basin and Range province (e.g., Cambray et al., 1995). Extension promotes formation of shallow chambers that have sheet-like morphology (Burov and Guillou-Frottier, 1999; Marti et al., 2000) that tend to evacuate almost entirely.

Zoning within Each Eruptive Unit at SWNVF and Time scales

Two end-member models are possible to explain the internal zoning in each tuff unit with respect to $\delta^{18}O$ (Fig. 5): either (1) they represent a single magma body that developed zoning in situ due to crystal fractionation and assimilation of country rocks having vertically different $\delta^{18}O$ values, or (2) rhyolitic and latitic portions represent two magmas (initially derived from a common parent) and having different $\delta^{18}O$ values that were brought into contact shortly prior to eruption.

In order to evaluate the first hypothesis, we performed mass balance calculations using Sr concentrations, $^{87}Sr/^{86}Sr_i$, $^{143}Nd/^{144}Nd$, and $\delta^{18}O$(melt). We used a variety of initial and boundary conditions (shown in Fig. 7) in an attempt to reconcile variations of these four parameters by an assimilation-fractional crystallization (AFC) model within a single magma chamber.

In all models, an initial lithosphere-derived basaltic magma containing 1000 ppm of Sr, 20–70 ppm Nd, with $^{87}Sr/^{86}Sr_I = 0.706$, $\varepsilon_{Nd} = -10$ to -13 (e.g., Farmer et al., 1991; DePaolo and Daley, 2000), and $\delta^{18}O$(melt) = 6.0‰ was taken as a mafic end-member. The silicic end-member contains either 300 or 30 ppm of Sr and 20–70 ppm Nd, and had $^{87}Sr/^{86}Sr_I = 0.720$, $^{143}Nd/^{144}Nd = 0.512$, and $\delta^{18}O$(melt) = 0‰, +5‰, and +10‰ (shown as stars in Fig, 7). The bulk D_{Sr} was taken to be 1.5, 2, 3, and 5. The basalt had initially high temperature (T) of 1320 °C, and T(assimilant) was at 500, 600, and 700 °C (Fig. 7, C-D). Assimilant had T(liquidus) = 900 °C and T(solidus) = 700 °C. It is important to stress that only these rather high initial temperatures yield meaningful AFC results (below), and they seem appropriate for high heat flux extensional terrain that additionally underwent previous magmatic pre-heating. The following observations put additional constraints on petrogenetic mechanisms.

(1) Chemical and isotopic zoning in tuffs could only be explained by either ''traditional'' or energy-constrained (Spera and Bohrson, 2001) AFC if there were high-$^{87}Sr/^{86}Sr_i$ (0.720), and low $^{143}Nd/^{144}Nd$ ($\varepsilon_{Nd} = -10$ to -13) assimilants. AT would require a moderately low-$\delta^{18}O$ (+4 to +5‰) silicic assimilant, and other tuffs would require high-$\delta^{18}O$ (+10‰) assimilant.

(2) Strong differences in both $^{87}Sr/^{86}Sr_I$ and 1/Sr between latites and rhyolites in each tuff unit (Fig. 7A) can only be reconciled if there were a low-Sr ($\sim$30 ppm), high-$^{87}Sr/^{86}Sr$ assimilant (>0.720), and extreme amounts of fractionation (approx. >95%). It is unlikely that such low-Sr rocks would constitute a majority of country rocks: high-$^{87}Sr/^{86}Sr$ end-members around SWNVF and elsewhere in the surrounding upper crust are represented by Precambrian granites ($^{87}Sr/^{86}Sr = 0.712$), but they contain 300 ppm Sr (Farmer et al., 1991). Additionally, AFC cannot explain the $^{87}Sr/^{86}Sr_i$ versus 1/Sr variations since they are perpendicular to the AFC trends.

(3) Purely on mass balance (''traditional'' AFC not shown), the $\delta^{18}O$(melt) versus $^{87}Sr/^{86}Sr_i$, and $^{87}Sr/^{86}Sr_i$ versus 1/Sr relations could explain the genesis of latites at moderate amounts of assimilation (25%–50%) but would require unreasonably large amounts of assimilation (>95%) to produce rhyolites. As a result, only a small residual volume of rhyolite would be produced. In contrast, rhyolites at SWNVF are the most voluminous magma type erupted.

(4) When the energy-constrained AFC model of Spera and Bohrson (2001) is employed (Fig. 7A-E), the AFC is even more restrictive and requires $\sim$75% crystallization of an initially hot 1320 °C basaltic magma and assimilant at high ambient temperature of 700 °C to generate latites. The 75% of AFC is more consistent with bulk melting of assimilants by the latent heat of mafic magma. Notice that the percentage of silicic magma produced after 75%–80% crystallization does not decrease further (Fig. 7, C-E). Most isotopic and chemical effects occur after 75% of this hypothetical AFC and are more consistent with progressive melting of country rocks (heat wave migration and zone refinement) than in an AFC process.

(5) Overall, the required strongly negative ε_{Nd} values (–12 to -9) for the inferred mafic magma end-member are similar to ε_{Nd} values measured in coeval mafic magmas in SWNVF and other lithosphere-derived intraplate mafic volcanics of the Great Basin (DePaolo and Daley, 2000; Miller et al., 2000). The AT magmas are 1–2 units higher in ε_{Nd} than the mafic end-member required for all other tuff units (see Fig. 5; Farmer et al., 1991), which is only possible to explain if the initial mafic magma had higher ε_{Nd} (Fig. 7E). Higher ε_{Nd} values for latites than for rhyolites in each tuff (especially in AT tuff) could be explained if latites contain a larger proportion of less negative ε_{Nd} basaltic component, achieved through its subsequent magma mixing with latites.

(6) The $\delta^{18}O$ values of silicic assimilant for AT should be no lower than 4–5‰ to fit the observed trends, and lower $\delta^{18}O$ values are not permissive (AS-2 but not AS-3, Fig, 7B). This observation alone suggests that >75% of silicic assimilant, most likely hydrothermally altered TS, TC, and RM cycle volcanics, should be present in the final AT magma, and again, 75% is more consistent with bulk melting rather than an AFC process.

Therefore, an AFC process in a single magma chamber cannot explain variations in $\delta^{18}O$(melt), $^{143}Nd/^{144}Nd$ (ε_{Nd}), $^{87}Sr/^{86}Sr_I$, and Sr, and is disproven based on heat and mass balance calculations. Large isotopic and chemical differences strongly suggest that latites and rhyolites represent different parental magmas.

Origin of Low-$\delta^{18}O$ Magmas at SWNVF: Comparison with Yellowstone

The genesis of voluminous low-$\delta^{18}O$ magmas at SWNVF has many similarities to that of less voluminous low-$\delta^{18}O$ magmas at Yellowstone. Both caldera complexes had low-$\delta^{18}O$ rhyolites that erupted <150 k.y. after caldera collapse. Another important similarity of SWNVF and Yellowstone is isotopically zoned zircons that have normal- to high-$\delta^{18}O$ cores in low-$\delta^{18}O$ magmas (Fig. 6), which are inherited from precaldera hydrothermally altered and $^{18}O/^{16}O$-depleted rocks.

High-$\delta^{18}O$ zircon (and quartz) xenocrysts can be explained by diffusive isotopic exchange with low-$\delta^{18}O$ melt (Fig. 8). At 850 °C and oxygen diffusion at water saturation

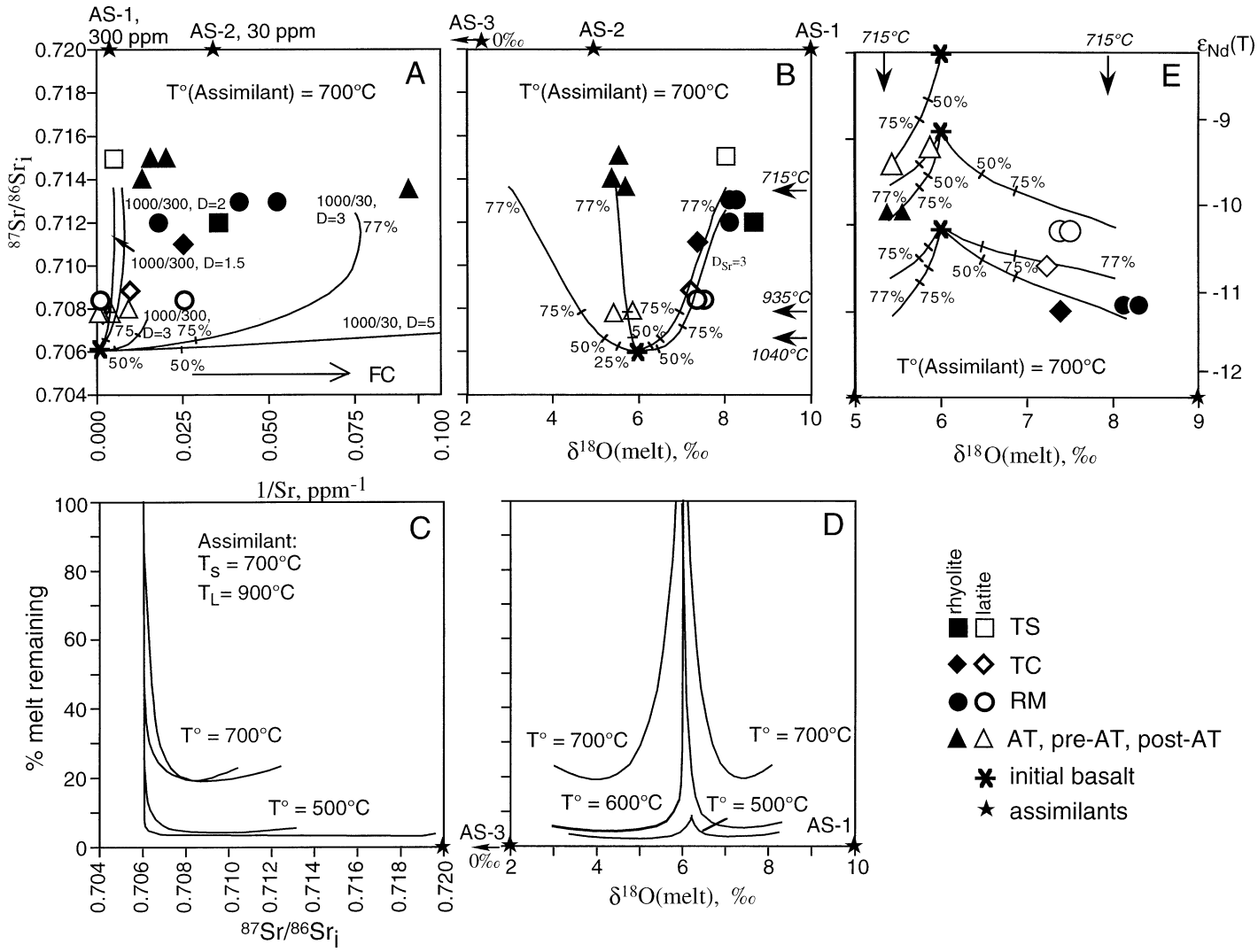

Figure 7. Values of $^{87}Sr/^{86}Sr_i$ vs. 1/Sr (A); $^{87}Sr/^{86}Sr_i$ vs. $\delta^{18}O$(melt) (B); percentage of melt remaining vs. $^{87}Sr/^{86}Sr_i$ (C), and $\delta^{18}O$(melt) (D), and $\varepsilon_{Nd}(t)$ vs. $\delta^{18}O$(melt) (E) based on energy-balanced assimilation-fractional crystallization (Spera and Bohrson, 2001) model curves. Tick marks on each curve represent proportion of magma crystallized. Notice that most isotopic and chemical effects occur after 75% crystallization, and this is more consistent with bulk melting of assimilant on a last stage of crystallization. Fractional crystallization (FC) alone does not change radiogenic isotope composition but decreases Sr (increases 1/Sr) concentration. FC causes subtle increase in $\delta^{18}O$(melt), taken to be ~0.3‰ per 80% fractionation (D, e.g., Harris et al., 2000). Comparison with SWNVF data demonstrates that chemical and isotopic contrast between rhyolites and latites of each unit is too great to be explained by a single AFC process. It is therefore unlikely that these variations are caused by an AFC process. Rhyolites and latites are best explained as two different magmas (see text for discussion).

(Farver and Yund, 1991; Watson and Cherniak, 1997), the remaining zoning in zircon and the lack of zoning in quartz in SWNVF would be consistent with their prolonged 10–15 k.y. residence in magma (see Bindeman and Valley, 2001 for further discussion on Yellowstone). Such a long time period would anneal all isotopic zonation in quartz and would partly anneal zonation in zircon. The 10–15 k.y. represents diffusion time that elapsed from immersion of normal-$\delta^{18}O$ zircons into molten low-$\delta^{18}O$ matrix melt, which approximates time from melting to eruption.

There are several differences between Yellowstone and SWNVF. At Yellowstone, low-$\delta^{18}O$ magmas appear as smaller intracaldera lava flows (<100 km^3), while low-$\delta^{18}O$ magmas at SWNVF are large and water-richer ash-flow sheets and lavas (>1000 km^3). The main difference between SWNVF and Yellowstone is that low-$\delta^{18}O$ magmas at Yellowstone are ultra low-$\delta^{18}O$ (down to ~0‰), while at SWNVF, magmas are moderately $^{18}O/^{16}O$ depleted (+5‰), which is possibly related to the higher $\delta^{18}O$ value of hydrothermally altered protolith (e.g., note AS-2 on Figure 7B) and much larger erupted volumes at SWNVF, suggesting that melting affected more variable and, on average, less ^{18}O-depleted sources.

The other difference is that at Yellowstone, low-$\delta^{18}O$ roof rocks were heated and remelted by the remaining silicic magma in a batholith-scale magma chamber after caldera collapse.

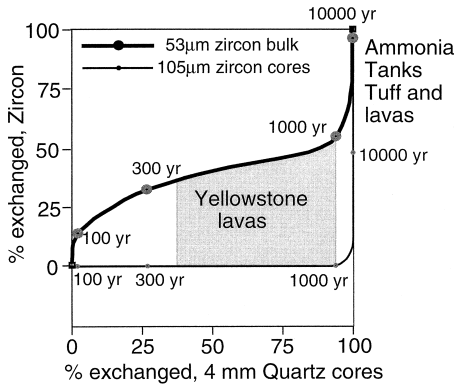

Figure 8. Isotopic exchange of quartz and zircon with low-$\delta^{18}O$ melt. Such exchange could result by rapid remelting of hydrothermally altered, low-$\delta^{18}O$ rocks in which quartz and zircon retained their initial normal-$\delta^{18}O$ values. Diffusion coefficients at 850 °C and P_{H2O} = 1 kb are from Watson and Cherniak (1997) for zircon and Farver and Yund (1991) for quartz. Notice the inflected curve for exchange of bulk of smaller (53 μm) zircons and L-shaped curve for zircon cores. The field for Yellowstone zircons and quartz is shown and requires 500–5000 yr of residence of xenocrysts in magma. In Ammonia Tanks tuff, $\delta^{18}O$(quartz) zoning is totally annealed, while the remaining subtle 0.5‰ zoning is consistent with 15,000–20,000 yr of residence at the same conditions. This model predicts that disequilibria due to unequal exchange between quartz and zircon would persist for up to 2000 yr; after that only zircon would show internal zoning lasting for up to 30,000 yr. Diffusion is assumed to become important when temperatures are raised during melting and to stop during eruption. The range of zircon zoning in Ammonia Tanks tuff is consistent with ~10,000 yr from melting to eruption. The range of zircon and quartz zoning in Yellowstone's low-$\delta^{18}O$ rhyolites is shown from Bindeman and Valley (2001) and is consistent with shorter residence times in smaller-volume low-$\delta^{18}O$ lavas.

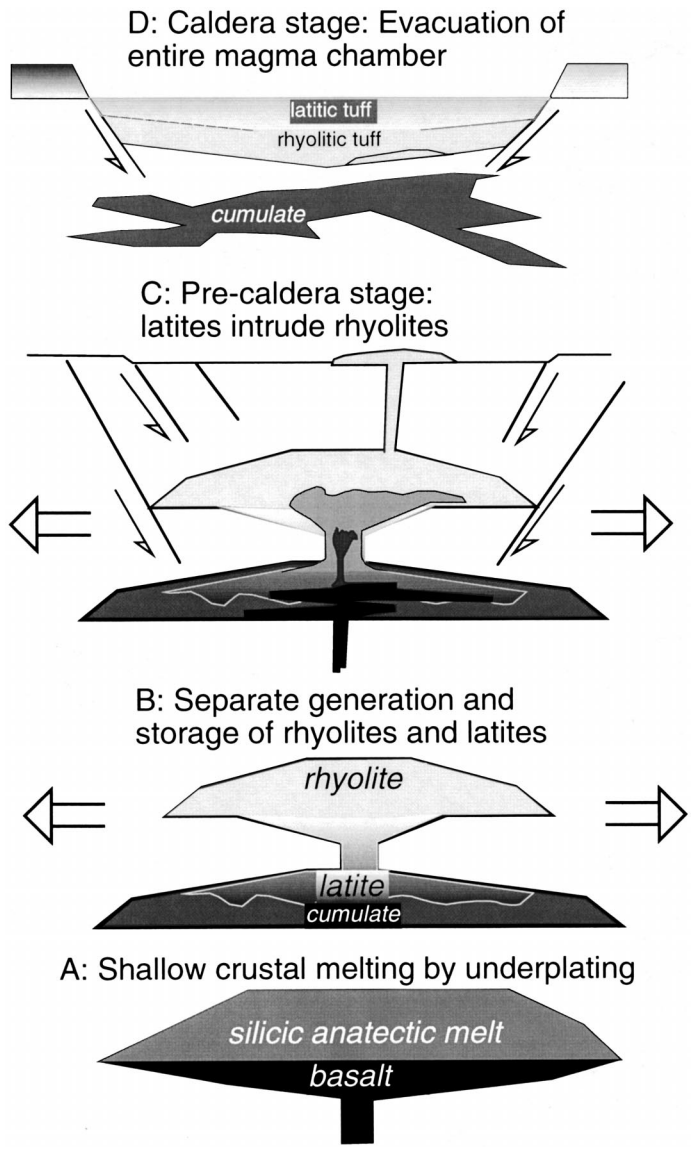

Figure 9. Magmatic evolution at SWNVF explaining evolutionary path for each ~100 k.y. cycle of volcanism. (A) Mid- to upper-crustal melting of variable-$\delta^{18}O$ crust by lithosphere-derived basalt in extensional environment of the Basin and Range province. (B) Formation of two vertically separated sheet-like magma chambers; rhyolites are separated upward from the silicic anatectic mush and acquired isotopic signatures of the upper crust; latites represent leftover cumulate-richer anatectic melt mixed with basalt. (C) Latites and more mafic magmas reintrude the upper rhyolitic magma chamber and occupy the lower part of the upper magma chamber, which leads to short-lived partial exchange of oxygen isotopes and trace elements through their interface shortly before the caldera-forming eruption. (D) Caldera-forming eruption evacuates the entire magma chamber.

At SWNVF, each magma body was evacuated during caldera formation. A new portion of mafic magma is necessary to melt hydrothermally altered rocks of the previous cycle, which were brought down with caldera collapse. Time scales are permissive. Roof melting by heat of freshly intruded mafic magma could be very rapid (thousands of years; e.g., Huppert and Sparks, 1988). Such rapid melting and eruption of entire magma bodies are consistent with Ar-Ar geochronology ($<10^5$ yr, Sawyer et al., 1994) and zoning profiles in zircons (10 k.y., Figs. 6, 8). Energy-constrained AFC calculations (Fig. 7) support the model of nearly complete bulk melting of crustal protholiths of varying $\delta^{18}O$ by heating of mafic magma. This, and the abundance of zoned zircons in AT, as well as its highly radiogenic nature, support the conclusion that most of AT is made of crustal melts. At Yellowstone, >50% of zircons in low-$\delta^{18}O$ rhyolites were derived from 0.1–2.0 m.y.—older precursor tuffs and lavas, as determined by in situ determinations of age and oxygen isotope ratios in zircons (Bindeman et al., 2001). We hypothesize by analogy with Yellowstone (pending SHRIMP dating at SWNVF) that

rocks of the AT cycle contain zircons that are derived from preceding 12.4–11.6 Ma hydrothermally altered tuffs and lavas of TS, TC, and RM cycles in the nested caldera complex of SWNVF.

The Petrogenesis of Zoned Tuffs at SWNVF

The genesis of each tuff unit can be explained by melting of either high-$\delta^{18}O$ rocks (such as RM and TS), more normal-$\delta^{18}O$ rocks (such as TC), or low-$\delta^{18}O$ rocks (such as AT on a >10 to <100 k.y. time scale). The heat of melting comes from freshly intruded basaltic magmas such that fill post-collapse caldera moats (Fig. 1), following solidification of evacuated magma chambers. Melting by moderately alkalic, lithospheric basalt (Fig. 9A) that has strongly negative ε_{Nd} produces silicic anatectic melt that has moderately alkalic affinity (e.g., Patiño Douce, 1999) and a composition likely to be intermediate between latite and rhyolites, as is also required by AFC modeling on Figure 7. We hypothesize that synmagmatic extension causes formation of two magma chambers (Fig. 9B). The crystal-rich latites can partly represent a leftover crystal mush in zones of melt generation in the lower magma chamber that experience a higher degree of subsequent hybridism and magma mixing with lithosphere-derived basaltic magma. Such interpretation is supported by petrographic and compositional data on the presence of fairly basic and mixed pumice in latites that have abundant and resorbed phenocrysts (Warren et al., 1989, 2000; Mills et al., 1997). Rhyolites could represent more evolved segregates that further fractionated and experienced assimilation of more radiogenic and higher-$\delta^{18}O$ plutonic and volcanic rocks at a shallower chamber by a process similar to zone refinement (e.g., Fig. 7), progressively losing contact with latites (Fig. 9B). Fractional crystallization in rhyolites is required by low Sr and very high Rb/Sr ratios in pre-AT rhyolites (Fig. 2A). Thus, we hypothesize that latites and rhyolites were separated vertically and acquired significant chemical and isotopic differences inherited from vertically variable country rocks. Latites reintruded the rhyolitic magma chamber prior to eruption (Fig. 9C). See Eichelberger et al. (2000) for a reverse configuration.

A model of short, possibly pre-eruptive reintrusion of latitic magma into rhyolite is most consistent with our data. Magmas were stratified according to density in an upper magma chamber without much mixing: The rhyolite occupied the upper portion in the magma chamber because it was crystal poor, volatile richer (Vogel and Aines, 1996), and less dense, and it erupted first. The coeval, crystal-rich, hot latitic magma with minor basaltic andesites was lower in the magma chamber and erupted later. The model of coeval eruption of two independent magmas also explains the 200 °C per 1–2.5 km temperature gradient, which could not persist in the pre-climactic magma chamber for 100 k.y. or even 10 k.y. Such thermal gradients in a shallow sheet-like magma chamber could not be sustained for an extended time without causing vigorous convection, which would average out thermal, chemical, and isotopic differences. Therefore, the time for two magmas to coexist was sufficiently short to prevent convective mixing and homogenization of $\delta^{18}O$ in the whole magma chamber. However, interface exchange of heat and some elements has taken place between rhyolitic and latitic magmas and accounts for the observed gradational transition from one composition to the other in each zoned ash-flow sheet. A model of layered convection having faster interface diffusion of heat, volatiles, alkalies, and trace elements (e.g., Sr and Nd), as compared to diffusion of major elements (e.g., Perez and Dunn, 1996; Bindeman and Davis, 1999), is capable of producing smooth, rather than step-function, gradients in the pre-climactic magma chamber.

A Note on Zoned Silicic Magma Systems

We presented oxygen isotope evidence of rapid generation and eruption of different $\delta^{18}O$ magmas. In contrast to Broxton et al. (1989), the inverted stratigraphy of four tuff units from SWNVF is not interpreted as a result of differentiation of a single, long-lived, chemically stratified silicic magma body. We consider that each tuff was initiated by intrusion of two magmas, rhyolitic and latitic, which are genetically related but segregated from different depths. After rhyolitic and latite magmas were juxtaposed in the same shallow magma chamber, they were stratified without much mixing and underwent limited thermal, chemical, and isotopic exchange though the interface up until eruption, but the exchange was not complete. This interpretation for the SWNVF may characterize similar extensional systems in the western United States and elsewhere. In other cases, however, oxygen-isotope evidence is consistent with an existence of a long-lived (10^5–10^6 yr) magma chambers where thermal, chemical, and isotopic gradients developed in situ after oxygen isotope equilibration (e.g., Bindeman and Valley, 2002). Thus, $\delta^{18}O$ of refractory minerals from caldera-forming eruptions serves as a powerful new tool in deciphering various mechanisms of magma segregation, assent, and eruption.

APPENDIX 1

Thermometry of Zoned Tuff Units

Zoned tuffs of SWNVF have been considered a classic example of temperature and compositional zoning (Lipman, 1971; Mills et al., 1997). Although Fe-Ti oxide geothermometry is widely used for determination of pre-eruptive temperature and oxygen fugacity, its use is limited because ilmenite is not always present in silicic volcanic rocks. In addition, exsolution of oxide minerals in some rocks may complicate successful application of Fe-Ti oxide geothermometry. Oxygen isotope fractionation between quartz and/or feldspar and magnetite can be more applicable for pyroclastic and effusive rocks because one or two of these mineral pairs are almost always present. It is important to determine to what extent postmagmatic processes (including oxyexsolution of ilmenite from magnetite) affect both oxygen isotopic exchange between magnetite and melt and isotopic temperatures.

Magnetite-ilmenite Oxide Thermometry

Magnetite and ilmenite in latitic and rhyolitic samples of each zoned tuff unit were analyzed by electron microprobe in order to determine temperature and oxygen fugacity (Ghiorso and Sack, 1991; Andersen and Lindsley, 1988). The analysis allows comparison of the oxygen isotope temperatures and magnetite-ilmenite temperatures for the same samples. Backscattered electron imaging of magnetite and ilmenite grain mounts revealed widespread oxyexsolution in magnetite. Ilmenite grains are more homogeneous and have no exsolution. The small (1-μm) scale of individual lamellae prevents their quantitative analysis and reconstruction of the bulk composition by reintegration using backscattered election (BSE) images (e.g., Cartwright et al., 1993). Instead, we chose to average multiple analyses (>30) made on a single grain with a wider beam (2–5 μm). Despite oxyexsolution in magnetite, most analyses obey the K(Mn/Mg) partitioning test between magnetite and ilmenite of Bacon and Hirschmann (1988), suggesting magmatic crystallization; a few individual spot analyses that did not adhere to the test were excluded. The degree of welding of tuff did not affect the estimated temperatures (Lipman, 1971). Analyses were made of 3–10 grains of ilmenite and magnetite in polished oxide grain mounts of each sample. A total of 1200 individual analyses was made of 10 samples (Fig. A1).

Oxygen Isotope Thermometry

Analyses of coexisting quartz, sanidine, and magnetite enable determination of Δ(Qz-Mt) and Δ(San-Mt) temperatures using the experimental calibrations of Chiba et al. (1989). Because minerals can exchange oxygen in subsolidus, the recognition of unaltered or minimally altered crystals is critical for correct temperature determination. The use of rapidly quenched pyroclastic rocks, such as the zoned tuffs of SWNVF or elsewhere, minimizes concerns of resetting. Air abrasion and small sample size for each analysis (1–2 mg), permit analyses of 3–10

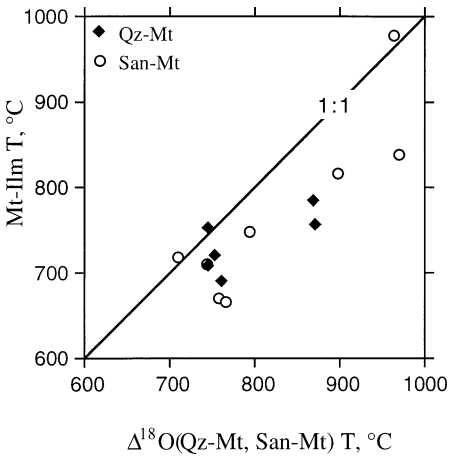

Figure A1. Isotope temperatures based on quartz-magnetite and sanidine-magnetite fractionations (Chiba et al., 1989; Clayton et al., 1989) compared to Fe-Ti oxides temperature of Ghiorso and Sack (1991). A line of 1:1 correspondence is shown. Andersen and Lindsley (1988) experimental calibration gives a similar result. Notice that isotope temperatures are systematically higher and are more consistent with liquidus relations; see text for further discussion.

fresh air-abraded cores. However, internal oxyexsolution in magnetite is present in almost all analyzed magnetites. They are likely to have formed on a magmatic stage still in the magma chamber (as evidenced by the above solidus Fe-Ti oxide temperatures) and do not reflect subsolidus oxyexsolution (in contrast to many plutonic and metamorphic rocks, e.g., Cartwright et al., 1993; Andersen and Lindsley, 1988). Addition of oxygen from melt or fluid during oxyexsolution will result in a change of the $\delta^{18}O$ value of the bulk grain, but the high temperature of such exchange, and similar value of $\delta^{18}O$(melt), will make this change small.

The calculated oxygen isotope temperatures are in the magmatic range of 700–900 °C (Fig. A1). Rhyolitic portions of each tuff demonstrate ~1‰ larger fractionations than for latitic portions, consistent with lower equilibration temperatures of rhyolites (Fig.A1). However, oxygen isotopic temperature is 50–100 °C higher than the magnetite-ilmenite temperature determined using either the Andersen and Lindsley (1988) or Ghiorso and Sack (1991) calibrations. The oxygen isotope temperatures are closer to what is expected for liquidus temperatures for both latite and rhyolites. Similar comparison of two thermometers was performed on fresher and younger Bishop Tuff, and yielded better correspondence (Bindeman and Valley, 2002). The discrepancies may be related to more resetting of magnetite-ilmenite due to exsolution and expulsion of ilmenite from magnetite grains. Thus, the use of quartz-magnetite and feldspar-magnetite isotope thermometry may be better preserved than the oxide geothermometry.

ACKNOWLEDGMENTS

We are grateful to John Fournelle for help with SEM and EMPA; to Mike Spicuzza for support during isotope analyses; to Drew Coleman, Steve Leedom, Bruce Hurley for help with sample collection; to Ryan Jakubowski and Julie O'Leary for help with mineral separation; and to Brian Hess for polishing thin sections and grain mounts. Jerry Szymanski assisted sampling of the fault gorge from Trench 14 at Yucca Mountain, and Rick Warren provided several important samples for this study, suggested localities to sample, and advised on tuff petrography. Reviews by Tom Vogel, Rick Warren, Lang Farmer, and extensive and helpful editorial suggestions by Lang Farmer and Allen Glazner are gratefully acknowledged. This research was supported by the U.S. Department of Energy under grant no. FGO2–93ER14389, DOE/NV/14389–2001–1.

REFERENCES CITED

Andersen, D.J., and Lindsley, D.H., 1988, Internally consistent solution models for Fe-Mg-Mn-Ti oxides: Fe-Ti oxides: American Mineralogist, v. 73, p. 714–726.

Bacon, C.R., and Hirschmann, M.M., 1988, Mg/Mn partitioning as a test for equilibrium between coexisting Fe-Ti oxides: American Mineralogist, v. 73, p. 57–61.

Bindeman, I.N., and Davis, A.M., 1999, Convection and redistribution of alkalis and trace elements during the mingling of basaltic and rhyolitic melts: Petrology, v. 7, no. 1, p. 91–101.

Bindeman, I.N., and Valley, J.W., 2000, Oxygen isotope study of accessory zircon, sphene and other minerals in carbonate cement of Trench 14, Yucca Mountain: No evidence for hydrothermal origin: Geological Society of America Abstracts with Programs, v. 33, p. 261.

Bindeman, I.N., and Valley, J.W., 2001, Low-$\delta^{18}O$ rhyolites from Yellowstone: Magmatic evolution based on analyses of zircons and individual phenocrysts: Journal of Petrology, v. 42, p. 1491–1517.

Bindeman, I.N., Valley, J.W., Wooden, J.L., and Persing, H.M., 2001, Postcaldera volcanism: In situ measurement of U-Pb age and oxygen isotope ratio in Pleistocene zircons from Yellowstone caldera: Earth and Planetary Science Letters, v. 189, p. 197–206.

Bindeman, I.N., and Valley, J.W., 2002, Oxygen isotope study of the Long Valley-Glass Mountain magmatic system, California: Isotope thermometry and convection in large silicic magma bodies: Contributions to Mineralogy and Petrology, v. 144, p. 185–205.

Broxton, D.E., Warren, R.G., Byers, F.M. Jr., and Scott, R.B., 1989, Chemical and mineralogic trends within the Timber Mountain-Oasis Valley caldera complex, NV: Evidence for multiple cycles of chemical evolution in a long-lived silicic magma system: Journal of Geophysical Research, v. 94, p. 5961–5985.

Burov, E.B., and Guillou-Frottier, L., 1999, Thermomechanical behavior of large ash flow calderas: Journal of Geophysical Research, v. 104, p. 23,081–23,109.

Byers, F.M., Jr., Carr, W.J., and Orkild, P.P., 1989, Volcanic centers of south-western Nevada: Evolution of understanding, 1960–1988: Journal of Geophysical Research, v. 94, p. 5908–5924.

Byers, F.M., Jr., Carr, W.J., Christiansen, R.L., Lipman, P.W., Orkild, P.P., and Quinlivan, W.D., 1976a, Volcanic suites and related cauldrons of Timber Mountain-Oasis valley caldera complex, Southern Nevada: U.S. Geological Survey Professional Paper, v. 919, 71p.

Byers, F.M., Jr., Carr, W.J., Orkild, P.P., Quinlivan, W.D., and Sargent, K.A., 1976b, Geologic map of the Timber Mountain caldera area, Nye County, Nevada: U.S. Geological Survey Miscellaneous Investigations Series, Map I-891, 1 sheet, 1: 100,000.

Cambray, F.W., Vogel, T.A., and Mills, J.G., Jr., 1995, Origin of compositional heterogeneities in tuffs of the Timber Mountain Group: The relationship between magma batches and magma transfer and emplacement in an extensional environment: Journal of Geophysical Research, v. 100, p. 15,793–15,805.

Cartwright, I., Valley, J.W., and Hazelwood, A.M., 1993, Resetting of oxybarometers and oxygen isotope ratios in granulite facies orthogneisses during cooling and shearing, Adirondack Mountains, New York: Contributions to Mineralogy and Petrology, v. 113, p. 208–225.

Chepizhko, A., Dublyansky, Y., and Szymanski, J., 1996, Hydrothermal accessory minerals in tuffs, creccias, and calcite/opal veins at Yucca Mountain, Nevada: TRAC-NA Final Report, submitted to Nuclear Waste Projects Office, State of Nevada, Contract 96/97.0009, 55 p.

Chiba, H., Chacko, T., Clayton, R.N., and Goldsmith, J.R., 1989, Oxygen isotope fractionations involving diopside, forsterite, magnetite, and calcite: Application to geothermometry: Geochimica et Cosmochimica Acta, v. 53, p. 2985–2995.

Christiansen, R.L., Lipman, P.W., Carr, W.J., Byers, F.M., Jr., Orkild, P.P., and Sargent, K.A., 1977, Timber Mountain-Oasis Valley caldera complex of southern Nevada: Geological Society of America Bulletin, v. 88, p. 943–959.

Clayton, R.N., Goldsmith, J.R., and Mayeda TK., 1989, Oxygen isotope fractionation in quartz, albite, anorthite and calcite: Geochimica et Cosmochimica Acta, v. 53, p. 725–733.

Crank, J., 1975, The mathematics of diffusion., 2nd ed. Clarendon Press, Oxford, 414 p.

Day, W.C., Potter, C.J., Sweetkind, D.S., Dickerson, R.P., and San-Juan, C.A., 1999, Bedrock geologic map of the central Block area, Yucca Mountain, Nye County, Nevada: U.S. Geological Survey Miscellaneous Investigations Series, Report I-2627.

DePaolo, D.J., and Daley, E.E., 2000, Neodymium isotopes in basalts of the southwest Basin and Range and lithospheric thinning during continental extension: Chemical Geology, v. 169, p. 157–185.

Dublyansky, Y.V., Szymanski, J.S., Chepizhko, A.V., Lapin, B.N., and Reutsky, V.N., 1998, Geological history of Yucca Mountain (Nevada) and the problem of a high-level nuclear waste repository, *in* Stenhouse, M.J., and Kirko, V.I., eds., Defense Nuclear Waste Disposal in Russia: Netherlands, Kluwer Academic Publishing, International Perspective, p. 279–292.

Dublyansky, Y.V., Ford, D., and Reutsky, V.N., 2001, Traces of epigenetic hydrothermal activity at Yucca Mountain, Nevada: Preliminary data on the fluid inclusion and stable isotope evidence: Chemical Geology, v. 173, p. 125–149.

Eichelberger, J.C., Chertkoff, D.G., Dreher, S.T., and Nye, C.J., 2000, Magmas in collision: Rethinking chemical zonation in silicic magmas: Geology, v. 28, p. 603–606.

Eiler, J.M., 2001, Oxygen isotope variations in basaltic lavas and upper mantle rocks, *in* Valley, J.W., and Cole, D.R., eds., Stable Isotope Geochemistry: Mineralogical Society of America, Reviews in Mineralogy, v. 43, p. 319–364.

Farmer, G.L., Broxton, D.E., Warren, R.G., and Pickthorn, W., 1991, Nd, Sr, and O isotopic variations in metaluminous ash-flow tuffs and related volcanic rocks at the Timber Mountain/Oasis Valley Caldera Complex, southwest Nevada: Implications for the origin and evolution of large-volume silicic magma bodies: Contributions to Mineralogy and Petrology, v. 109, p. 53–68.

Farver, J.R., and Yund, R.A., 1991, Oxygen diffusion in quartz: dependence on temperature water fugacity: Chemical Geology, v. 90, p. 55–70.

Flood, T.P., Vogel, T.A., and Schuraytz, B.C., 1989, Chemical evolution of a magmatic system: The Paintbrush tuff, southwest Nevada volcanic field: Journal of Geophysical Research, v. 94, p. 5943–5960.

Friedman, I., Lipman, P.W., Obradovich, J.D., Gleason, J.D., and Christiansen, R.L., 1974, Meteoric water in magmas: Science, v. 184, p. 1069–1072.

Frizzell, V.A., Jr., and Shulters, J.C., 1990, Geologic map of the Nevada Test Site, southern Nevada: U.S. Geological Survey Miscellaneous Investigations Series, Map I-2046, 1: 100,000.

Ghiorso, M.S., and Sack, R.O., 1991, Fe-Ti oxide geothermometry—thermodynamic formulation and the estimation of intensive variables in silicic magmas:

Contributions to Mineralogy and Petrology, v. 108, p. 485–510.

Huppert, H.E., and Sparks, R.S.J., 1988, Melting the roof of a chamber containing a hot turbulently convective fluid: Journal of Fluid Mechanics, v. 188, p. 107–131.

Harris, C., Smith, H.S., and le Roex, A.P., 2000, Oxygen isotope composition of phenocrysts from Tristan da Cunha and Gough Island lavas: Variations with fractional crystallization and evidence for assimilation: Contributions to Mineralogy and Petrology, v. 138, p. 164–175.

Huysken, K.T., Vogel, T.A., and Layer, P.W., 1994, Incremental growth of a large-volume, chemically zoned magma body—a study of the tephra sequence beneath the Rainier Mesa ash-flow sheet of the Timber Mountain tuff: Bulletin of Volcanology, v. 56, p. 377–385.

Huysken, K.T., Vogel, T.A., and Layer, P.W., 2001, Tephra sequences as indicators of magma evolution: Ar-40/Ar-39 ages and geochemistry of tephra sequences in the southwest Nevada volcanic field: Journal of Volcanology and Geothermal Research, v. 106, p. 85–110.

King, E.M., Valley, J.W., Davis, D.W., and Kowalis, B.J., 2001, Empirical determination of oxygen isotope fractionation factors for titanite with respect to zircon and quartz: Geochimica et Cosmochimica Acta, v. 65, p. 3165–3175.

Lipman, P.W., 1971, Iron-titanium oxide phenocrysts in compositionally zoned ash-flow sheets from southern Nevada: Journal of Geology, v. 79, p. 438–456.

Lipman, P.W., 1984, The roots of ash-flow calderas in the western North America: Windows in to the tops of granitic batholiths: Journal of Geophysical Research, v. 89, p. 8801–8841.

Lipman, P.W., and Friedman, I., 1975, Interaction of meteoric water with magmas: An oxygen isotope study of ash-flow sheets from southern Nevada: Geological Society of America Bulletin, v. 86, p. 695–702.

Lipman, P.W., Christiansen, R.L., and O'Connor, J.T., 1966, A compositionally-zoned ash-flow sheet in southern Nevada: U.S. Geological Survey Professional Paper 524-F, p. 1–47.

Marti, J., Folch, A., Neri, A., and Macedonio, G., 2000, Pressure evolution during explosive caldera-forming eruptions: Earth and Planetary Science Letters, v. 175, p. 275–287.

Matthews, A., Palin, J.M., Epstein, S., and Stolper, E.M., 1994, Experimental-study of $^{18}O/^{16}O$ partitioning between crystalline albite, albitic glass, and CO_2 gas: Geochimica et Cosmochimica Acta, v. 58, p. 5255–5266.

Marshall, B.D., Kyser, T.K., and Peterman, Z.E., 1996, Oxygen isotopes and trace elements in the Tiva Canyon tuff, Yucca Mountain and vicinity, Nye County, Nevada: U.S. Geological Survey Open File Report 95–0431, 49 p.

Miller, J.S., Glazner, A.F., Farmer, G.L., Suayah, I.B., and Keith, L.A., 2000, A Sr, Nd, and Pb isotopic study of mantle domains and crustal structure from Miocene volcanic rocks in the Mojave Desert, California: Geological Society of America Bulletin, v. 112, p. 1264–1279.

Mills, J.G., Jr., Saltoun, B.W., and Vogel, T.A., 1997, Magma batches in the Timber Mountain magmatic system, southwest Nevada volcanic field, Nevada, USA: Journal Volcanology and Geothermal Research, v. 78, p. 185–208.

Morishita, Y., Giletti, B.J., and Farver, J.R., 1996, Volume self-diffusion of oxygen in titanite: Geochemical Journal, v. 30, p. 71–79.

Neymark, L.A., Marshall, B.D., Kwak, L.M., Futa, K., and Mahan, S.A., 1995, Geochemical and Pb, Sr, and O isotopic study of the Tiva Canyon tuff and Topopah Spring tuff, Yucca Mountain, Nye County, Nevada: U.S. Geological Survey Open File Report 95–134, 18 p.

Noble, D.C., and Hedge, C.E., 1969, $^{87}Sr/^{86}Sr$ variation within individual ash-flow sheets, U.S. Geological Survey Professional Paper, v. 65-C, p. 133–139.

Palin, J.M., Epstein, S., and Stolper, E.M., 1996, Oxygen isotope partitioning between rhyolitic glass/melt and CO_2: An experimental study at 550–950 °C and 1bar: Geochimica et Cosmochimica Acta, v. 60, p. 1963–1973.

Patiño Douce, A.E., 1999, What experiments tell us about the relative contributions of crust and mantle to the origin of granitic magmas, *in* Castro, A., ed., Understanding granites; integrating new and classical techniques: Geological Society [London] Special Publications, v. 168, p. 55–75.

Perez, W.A., and Dunn, T., 1996, Diffusivity of Sr, Nd, and Pb in natural rhyolite at 1 Gpa: Geochimica et Cosmochimica Acta, v. 60, p. 1387–1397.

Rumble, D., 1992, A review of the isotope geochemistry of the Yucca Mountain, Nevada, proposed Nuclear Waste Repository site, *in* Ground water at Yucca Mountain: How high can it rise: Washington D.C., National Research Council, p. 147–171.

Sawyer, D.A., Fleck, R.J., Lanphere, M.A., Warren, R.G., Broxton, D.E., and Hudson, M.R., 1994, Episodic caldera volcanism in the Miocene southwest Nevada volcanic field: Related stratigraphic framework, $^{40}Ar/^{39}Ar$ geochronology, and implications for magmatism and extension: Geological Society of America Bulletin, v. 106, p. 1304–1318.

Schuraytz, B.C., Vogel, T.A., and Younker, L.W., 1989, The Topopah Spring tuff: Evidence for dynamic withdrawal from a layered magma body: Journal of Geophysical Research, v. 94, p. 5925–5942.

Spera, F.J., and Bohrson, W.A., 2001, Energy-constrained open-system magmatic processes I: General model and energy-constrained assimilation-fractional crystallization (EC-AFC) formulation: Journal of Petrology, v. 42, p. 999–1018.

Spicuzza, M.J., Valley, J.W., Kohn, M.J., Girard, J.P., and Fouillac, A.M., 1998a, The rapid heating, defocused beam technique: A CO_2 -laser-based method for highly precise and accurate determination of $\delta^{18}O$ values of quartz: Chemical Geology, v. 144, p. 195–203.

Spicuzza, M.J., Valley, J.W., and McConnell, V.S., 1998b, Oxygen isotope analysis of whole rocks via laser fluorination: An airlock approach: Geological Society of America Abstracts with Programs, v. 30, p. 80.

Stolper, E.M., and Epstein, S., 1991, An experimental study of oxygen isotope partitioning between silica glass and CO2 vapor, *in* Taylor, H.P., O'Neil, J.R., and Kaplan, I.R., eds.: Geochemical Society Special Publication N3, p. 35–51.

U.S. Department of Energy, 1993, Report on the origin of calcite-silica deposits at Trench 14 and Busted Butte and methodologies used to determine their origin: Las Vegas, Nevada, Office of Civilian Radioactive Waste Management, 120 p.

Valley, J.W., Kitchen, N., Kohn, M.J., Niendorf, C.R., and Spicuzza, M.J., 1995, UWG-2, a garnet standard for oxygen isotope ratio: Strategies for high precision and accuracy with laser heating: Geochimica et Cosmochimica Acta, v. 59, p. 5223–5231.

Valley, J.W., Bindeman, I.N., and Peck, W.H., 2003, Empirical calibration of oxygen isotope fractionations in zircon: Geochimica et Cosmochimica Acta, (in press).

Vogel, T.A., and Aines, R., 1996, Melt inclusions from chemically zoned ash-flow sheets from the southwest Nevada volcanic field: Journal of Geophysical Research, v. 101, p. 5591–5610.

Warren, R.G., Byers, F.M., Jr., Broxton, D.E., Freeman, S.H., and Hagan, R.C., 1989, Phenocryst abundances and glass and phenocrysts compositions as indicator of magmatic environments of large volume ash-flow sheets in southwestern Nevada: Journal of Geophysical Research, v. 94, p. 5987–6020.

Warren, R.G., Sawyer, D.A., Byers, F.M., Jr., and Cole, G.L., 2000, A petrographic/geochemical database and stratigraphic framework for the southern Nevada volcanic field: Los Alamos Report: http://queeg.ngdc.noaa.gov/seg/geochem/swnvf/.

Watson, E.B., and Cherniak, D.J., 1997, Oxygen diffusion in zircon: Earth and Planetary Science Letters, v. 148, p. 527–544.

Watson, E.B., and Harrison, T.M., 1983, Zircon saturation revisited: Temperature and compositional effects in a variety of crustal magma types: Earth and Planetary Science Letters, v. 64, p. 295–304.

Xirouchakis, D., and Lindsley, D.H., 1998, Equilibria among titanite, hedenbergite, fayalite, quartz, ilmenite, and magnetite: Experiments and internally consistent thermodynamic data for titanite: American Mineralogist, v. 83, p. 712–725.

Zhang, X.Y., Cherniak, D.J., and Watson, E.B., 2001, Preliminary experimental results for oxygen diffusion in titanite under anhydrous conditions: Geological Society of America Abstracts with Programs, v. 33, p. 238.

MANUSCRIPT RECEIVED BY THE SOCIETY 27 DECEMBER 2001
REVISED MANUSCRIPT RECEIVED 24 SEPTEMBER 2002
MANUSCRIPT ACCEPTED 10 OCTOBER 2002

Printed in the USA

Data Repository item 2003066: Minerals in carbonate cement of Yucca Mountain

There have been reports of hydrothermal zircon and sphene in carbonate cements filling faults in and around Yucca Mountain (Dublyansky et al., 1998; Chepizhko et al., 1996), in particular in well-studied Trench 14. The existence of hydrothermally-precipitated zircons and sphenes would have implications for our use of zircon chemistry to study magmatic evolution and also for the Yucca Mountain Repository. Trench 14 traverses the Bow Ridge Fault which is a normal fault with a near-vertical displacement of 190 meters separating exposures of Rainier Mesa and Tiva Canyon tuffs (Report, 1993). Proving the hydrothermal origin of sphene and zircon in carbonate cement would indicate a relatively high temperature of hydrothermal solution that is pertinent to the risk assessment at Yucca Mountain. If hydrothermal, these zircons and sphenes can be used for successful U-Pb dating Single crystal SIMS or TIMS), and thus the age of last hydrothermal activity could be determined. We dissolved 5kg of carbonate-cemented fault gorge material from Trench 14 in HCl. Dr. Jerry Szymanski assisted in sampling from Trench 14 to ensure that our material was the same as that studied by Dublyansky et al. 1998) and Chepizhko et al. (1996). Extracted silicate fragments are represented by vesicular pumice clasts (>50wt% of the total mass), and individual minerals preserving igneous morphology.

Analyses of zircon, sphene, quartz, sanidine, pyroxene, amphibole, magnetite, and glass extracted from the carbonate cement of Trench 14 were performed individually or in bulk (Table 2). The oxygen isotope ratios of analyzed minerals, and the small mineral-mineral fractionations are consistent with high magmatic temperatures. The ^{18}O of extracted zircons is +6.35‰ consistent with mixture of igneous zircons from the Rainier Mesa (+6.54 to 6.61‰) and Tiva Canyon tuffs (+5.68 to 5.93‰) (Fig. A2). The ^{18}O value of sphene is 4.03‰, close to that of Tiva Canyon tuff (+4.74 to 4.76‰). Magnetite is 2.62‰, similar to RM (+2.5 to 3‰) and TC (+2.16 to 3.56‰), a piece of brown glass is 8.03‰, and 1 individual sanidine crystal is 7.90‰ similar to that in RM (San = +8‰), green clinopyroxene is 5.65‰, black amphibole is 5.00‰, also similar to TC or RM.

If any of the analyzed silicate minerals were precipitated from hydrothermal fluid, then they should be related to the ^{18}O values of the fluid at respective temperatures of exchange (Fig. A2). For example, mineral-water oxygen isotope fractionation (Zheng, 1993) at >25 ^{0}C with ^{18}O(water) = -10‰, -14‰, -18‰ consistent with equilibrium with: calcite cement, present-day groundwater, and Pleistocene groundwater respectively (Rumble, 1992) would generate lower ^{18}O values of hydrothermally-precipitated zircon, sphene, and other minerals, than is observed in Trench 14. For example, at 50° C hydrothermal zircons will have ^{18}O<0‰, and negative values at higher T. In addition, the fractionation between different minerals would be larger than observed.

We conclude that analyzed silicate and oxide minerals and glass from the carbonate cement Trench 14 are magmatic in origin and that fluids responsible for deposition of carbonate did not exchange oxygen with silicate material. Extracted minerals and glass represent tectonically-crushed and variably ground Rainier Mesa and Tiva Canyon tuffs, to the level of individual phenocrysts. These results do not support previous reports of hydrothermally precipitated zircon and sphene in Trench 14, and they support our conclusion that zircons faithfully preserve magmatic composition.

Fig. A2 Captions:
Fig. A2 A: Comparison of ^{18}O values of minerals in carbonate cement of Trench 14 through Bow Ridge fault of Yucca Mountain and those in Tiva Canyon and Rainier Mesa tuffs, that form lower and upper shoulders of the fault. Notice that mineralogy and ^{18}O of crystals within carbonate cement can be explained by mechanical mixture of tuffs adjacent to fault.
B-C: Calculated values of ^{18}O(Zrc), A2B, and ^{18}O(Sphene), A2C, in equilibrium with water of different ^{18}O values and temperatures. Zircon and Sphene-water fractionations are calculated using experimental quartz-water (Friedman and O'Neil, 1977) and empirical quartz-sphene (King et al., 2001) and quartz-zircon (Valley et al. 2003).

Appendix 2 additional references.

Friedman, I., O'Neil, J.R., 1977, Compilation of stable isotope fractionation factors of geochemical interest: U.S. Geological Survey Professional Paper 440-KK.

Zheng, Y.F., 1993, Calculation of oxygen isotope fractionation in anhydrous silicate minerals, Geochimica et Cosmochimica Acta, v. 57, p. 1079-1091.

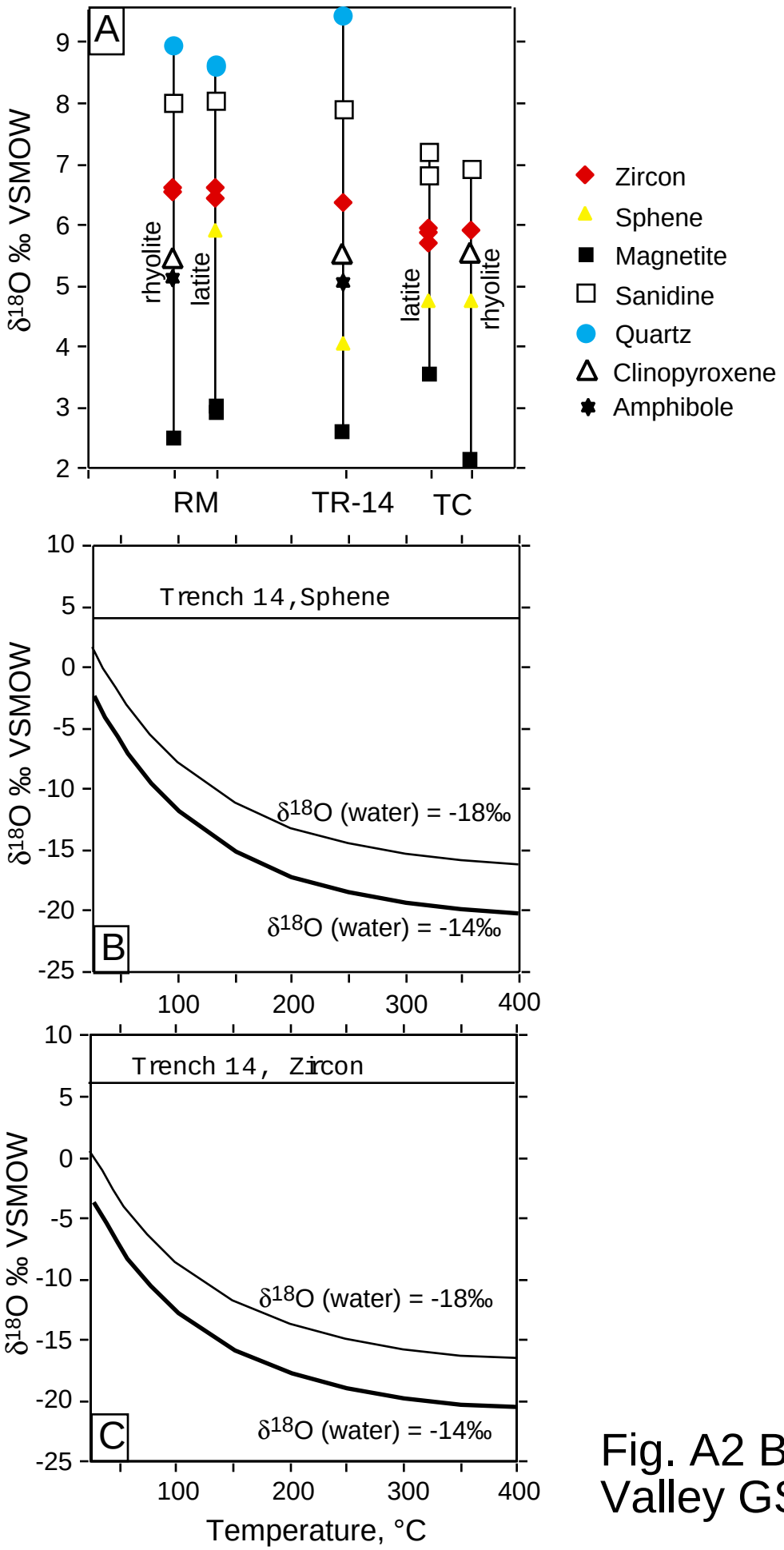

Fig. A2 Bindeman and Valley GSA Bulletin